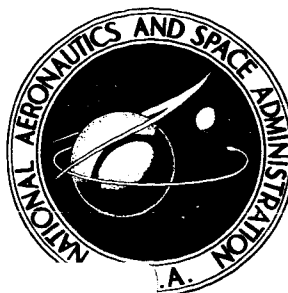


**NASA CONTRACTOR
REPORT**



NASA CR-153

NASA CR-153

N65 14116
(ACCESSION NUMBER)
76
(PAGES)
CR-153
(NASA CR OR TMX CR AD NUMBER)

(THRU)
1
(CODE)
30
(CATEGORY)

GPO PRICE \$ _____

OTS PRICE(S) \$ *3.00*

Hard copy (HC) _____

Microfiche (MF) *.75*

HODOGRAPH ANALYSIS OF THE FREE-FLIGHT TRAJECTORIES BETWEEN TWO ARBITRARY TERMINAL POINTS

by Fang Tob Sun

Prepared under Grant No. NsG-558 by

UNIVERSITY OF MICHIGAN

Ann Arbor, Mich.

for

NATIONAL AERONAUTICS AND SPACE ADMINISTRATION • WASHINGTON, D. C. • JANUARY 1965

HODOGRAPH ANALYSIS OF THE FREE-FLIGHT TRAJECTORIES
BETWEEN TWO ARBITRARY TERMINAL POINTS

By Fang Toh Sun

Distribution of this report is provided in the interest of information exchange. Responsibility for the contents resides in the author or organization that prepared it.

Prepared under Grant No. NsG-558 by
UNIVERSITY OF MICHIGAN
Ann Arbor, Michigan

for

NATIONAL AERONAUTICS AND SPACE ADMINISTRATION

For sale by the Office of Technical Services, Department of Commerce,
Washington, D.C. 20230 -- Price \$3.00

ABSTRACT

14116

An analytic treatment of the free-flight trajectories between two terminal points in space by using the hodograph method is presented. A general case is assumed in which the range angle and the terminal distances from the field center are both arbitrary, and all three possible types of the Keplerian trajectories, the elliptic, the parabolic, and the hyperbolic, are considered. A single representation of the infinitely many such trajectories in a dimensionless hodograph plane is introduced, and a general survey of such trajectory system as seen from the hodograph is made. By using the hodograph geometry the characteristics of the conjugate trajectories are explored; and in line with this the minimum energy trajectory is briefly reviewed. Besides, the existence of a least eccentric trajectory for given terminal points is proved, and its characteristics briefly analyzed. Several sets of general formulas for the principal elements of such terminal-constrained trajectories are also presented, including some explicit expressions for the terminal path angles. No particular trajectory problems are discussed; as a general analysis, it is intended to provide some basis for the analytic treatment of such problems, especially those of trajectory optimization and selection in free-flight.

Author

TABLE OF CONTENTS

	Page
LIST OF TABLES	vii
LIST OF FIGURES	viii
NOMENCLATURE	ix
I. INTRODUCTION	1
II. HODOGRAPHIC REPRESENTATION AND GENERAL SURVEY OF THE SYSTEM OF CO-TERMINAL TRAJECTORIES	2
General Considerations	2
The Hodographic Representation	4
A General Survey	6
Limits of Variation of the Trajectory Elements	9
III. THE CHORDAL AND RADIAL COMPONENTS OF THE TERMINAL VELOCITIES	15
IV. CHARACTERISTICS OF THE CONJUGATE TRAJECTORIES	18
V. THE PRINCIPAL ELEMENTS OF THE CONJUGATE TRAJECTORIES	25
VI. ANALYSIS OF SOME PARTICULAR TRAJECTORIES	31
The Minimum Energy Trajectory	31
The Least Eccentric Trajectory and Its Conjugate	35
Other Trajectories	37
VII. THE CASE OF 180 DEGREE RANGE	39
Hodographic Representation and General Survey	39
The Characteristics of the Conjugate Trajectories and Their Principal Elements	42
The Minimum Energy Trajectory and the Least Eccentric Trajectory	46
VIII. SUMMARY OF CONCLUSIONS	61

TABLE OF CONTENTS (Concluded)

	Page
APPENDICES	
A. CORRELATIONS BETWEEN THE PHYSICAL PLANE AND THE HODO- GRAPH PLANE FOR THE KEPLERIAN ORBITS	64
B. SUMMARY OF FORMULAS: DURATION OF TERMINAL-TO-TERMINAL FLIGHT	65
REFERENCES	66

LIST OF TABLES

Table	Page
1. Location of the Hodograph Origin and the Nature of the Terminal-Constrained Trajectory	8
2. Possible and Forbidden Regions of Departure and Approach	13
3. Regions for the Apsidal Axes (Positive Portion)	14
4. Formulas for the Principal Elements of the Conjugate Trajectories	27
5. Hodographic Criteria for the Occurrence of Apses on the Trajectory	30
6. Possible and Forbidden Regions of Departure and Approach, 180° Range	41

LIST OF FIGURES

Figure		Page
1	System of co-terminal trajectories and its hodographic representation (range $\neq 180^\circ$).	3
2	Proof of the linear distribution of the hodograph origins.	5
3	General survey of the system of co-terminal trajectories.	10
4	Terminal velocities and their chordal and radial components.	16
5-1	The conjugate elliptic trajectories, range $< 180^\circ$.	20
5-2	The conjugate hyperbolic trajectories, range $< 180^\circ$.	21
5-3	The conjugate parabolic trajectories, range $< 180^\circ$.	22
6	The minimum energy trajectory and its relation with a pair of conjugate trajectories, range $< 180^\circ$.	32
7	The least eccentric trajectory and its conjugate, range $< 180^\circ$.	36
8	System of co-terminal trajectories and its hodographic representation, 180° range.	40
9-1	The conjugate elliptic trajectories, 180° range.	44
9-2	The conjugate hyperbolic trajectories, 180° range.	45
10	The minimum energy and least eccentric trajectory, 180° range.	47
11-1	Variation of the range-constrained path angle with distance ratio and initial speed: a. $\psi = 60^\circ$ b. $\psi = 90^\circ$ c. $\psi = 120^\circ$ d. $\psi = 180^\circ$	49
11-2	Variation of the range-constrained trajectory eccentricity with distance ratio and initial speed: a. $\psi = 60^\circ$ b. $\psi = 90^\circ$ c. $\psi = 120^\circ$ d. $\psi = 180^\circ$	53
11-3	Variation of the duration of terminal-to-terminal flight with distance ratio and initial speed: a. $\psi = 60^\circ$ b. $\psi = 90^\circ$ c. $\psi = 120^\circ$ d. $\psi = 180^\circ$	57

NOMENCLATURE

- a semimajor axis, elliptic trajectory; or semitransverse axis, hyperbolic trajectory
- b semiminor axis, elliptic trajectory; or semiconjugate axis, hyperbolic trajectory
- c focus-to-center distance, conic orbit
- d base altitude, the perpendicular distance from the field center to the chord
- g gravitational acceleration
- h angular momentum per unit mass
- k orbital energy per unit mass
- l chord length
- M gravitating mass
- m l/r_1
- n r_2/r_1
- r radial distance
- \bar{r} semilatus rectum
- s semi-perimeter of the base triangle
- t time
- V speed
- \vec{V} velocity vector
- x,y rectangular coordinates
- \dot{x}, \dot{y} rectangular velocity coordinates
- \hat{x}, \hat{y} dimensionless velocity coordinates $= (h/\mu) \dot{x}, (h/\mu) \dot{y}$

NOMENCLATURE (Continued)

- γ half-angle between the asymptotes, hyperbolic orbit, defined in Appendix A
- δ inclination of the line of origins, defined in Figure 1b
- e eccentricity of the trajectory
- ζ, χ parameters, defined by Eq. (31)
- θ true anomaly
- κ parameter, defined by Eq. (52)
- λ speed parameter = V/V^*
- μ strength of the gravity field = Mg
- ξ_0, η_0 Lamberts parameters, elliptic trajectory, defined in Appendix B
- ξ'_0, η'_0 Lamberts parameters, hyperbolic trajectory, defined in Appendix B
- τ period of elliptic motion
- Φ auxiliary angle, defined in Figures 5-1,2,3
- ϕ path angle with respect to local horizon
- φ base angle, the interior angle of the base triangle at the terminal point
- ψ vertex angle, the interior angle of the base triangle at the field center, or the range angle of the normal trajectory
- ψ' range angle of the complementary trajectory = $2\pi - \psi$
- ω auxiliary angle, defined in Figure 3

Subscripts

- 1 initial terminal
- 2 final terminal

NOMENCLATURE (Concluded)

- I low trajectory
- II high trajectory
- A apocenter
- P pericenter
- e elliptic
- h hyperbolic
- UL upper limit
- LL lower limit
- C,R chordal and radial components
- θ, r transversal and radial components
- ∞ trajectory of infinite speed
- ' complementary trajectory
- * minimum energy trajectory

Superscript

- * escape or parabolic

I. INTRODUCTION

In recent years the problems of orbital transfer have been under extensive study; in the meantime, following the emergence of long-range missiles, ballistic analysis has extended from artillery trajectories to space trajectories. In essence the free-flight trajectories being dealt with in both classes of problems are the same, all belong to the so-called Keplerian conics. In ballistic analysis, usually the elliptic trajectories are the focus of attention, and most analyses emphasize the symmetrical case, that is, the two terminal points are assumed to be equi-distant from the center of the gravity field, leaving the class of parabolic or hyperbolic trajectories, and the unsymmetrical case either ignored or barely touched. In orbital transfer problems such as those in interplanetary flight, more varieties in the type of trajectory and terminal conditions are encountered; however, most studies were in the area of optimization rather than in the characteristics of the possible transfer trajectories themselves. Furthermore, despite the fact that the mechanics of Keplerian motion has been well known and amenable to complete analysis, characteristics of Keplerian trajectories, especially those under terminal constraints, have not been fully explored; and the existing trajectory formulas are not all adequate.

In view of this situation a unified treatment of the free-flight trajectories of all three types of the Keplerian conics between two arbitrary terminal points in space is presented so as to provide a basis for further analysis and selection of particular trajectories in either class of problems, the ballistic missile flight or the orbital transfer, or any relevant ones in which such trajectories are involved (such as satellite rendezvous and ballistic return). As a basic analysis, whether these terminal points are situated on given orbits or not is immaterial.

Throughout this paper instead of using the Wheelon's hit equation⁴ as usually employed, the treatment is made mainly by the hodograph method, which is not only suitable for such unified treatment, but also helps to bring out many essential features of such system of co-terminal trajectories by bypassing many mathematical complexities through the geometrical approach in the hodograph plane. The results of such analysis also lead to several sets of general formulas for the elements of such trajectories which might supplement the existing ones. Such hodograph method is based on the author's previous work contained mainly in Ref. 8, some essential materials of which are condensed in Appendix A for reference.

II. HODOGRAPHIC REPRESENTATION AND GENERAL SURVEY OF THE SYSTEM OF CO-TERMINAL TRAJECTORIES

GENERAL CONSIDERATIONS

In a central force field all free-flight trajectories passing through two fixed terminal points, Q_1 and Q_2 will lie in the same plane determined by the three points Q_1 , Q_2 , and the field center O . The triangle OQ_1Q_2 will be called the base triangle; the base Q_1Q_2 , the chord; and the interior angle at O , the vertex angle. The initial velocity vector to achieve such trajectory will necessarily be coplanar with the base triangle, while either its magnitude or its direction in the trajectory plane may be arbitrary. Thus in a given force field the geometry of the base triangle together with the initial speed or the initial path angle completely determine the trajectory. If the field is Newtonian, then the trajectory is known as Keplerian, which will be elliptic, parabolic, or hyperbolic according as the initial speed parameter λ_1 is smaller than, equal to, or greater than unity, where by definition,

$$\lambda = \frac{V}{V^*} = \frac{V}{\sqrt{2\mu/r}} . \quad (1)$$

A typical base triangle and several such Keplerian trajectories are depicted in Figure 1(a). The geometry of such trajectory system in the physical plane has been analyzed to some detail by Battin.³ The purpose of this section is to represent such system in the hodograph plane so as to form the basis for subsequent analysis.

It is to be noted that, with two given terminals, a vehicle starting from one terminal may reach the other in either direction around the field center. Thus the system of co-terminal trajectories may be divided into two groups: the one with a common range angle equal to the vertex angle ψ which is less than π , and the other with a common range angle $\psi' = 2\pi - \psi$ which is greater than π . The first group is usually the one of interest in most practical problems, and will be called the normal group, while the second, its complement. In fact each member of one group will find its complement in the other, the two forming a complete Keplerian conic. However, if the trajectory is parabolic or hyperbolic, then its complement, being open between the terminals, can hardly be regarded as a trajectory in the ordinary sense, and will be referred to as an unrealistic trajectory for convenience. In the following the main analysis will be concerned with the trajectory system of the normal group with $\psi < \pi$. However, as we will see, the informations so obtained may be easily adapted to its complementary group if needed. The boundary case of $\psi = \pi$ will be treated separately later.

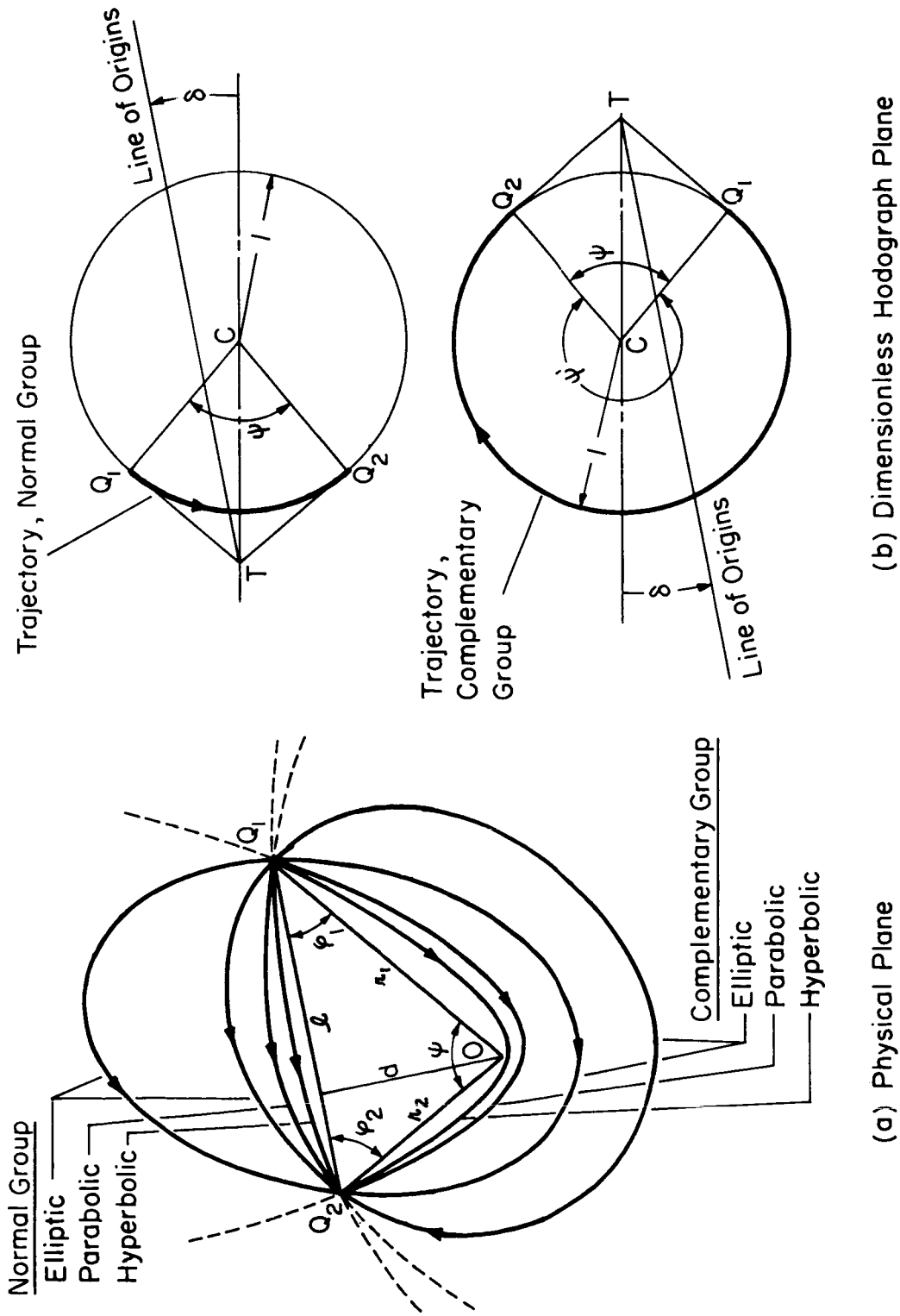


FIGURE 1. SYSTEM OF CO-TERMINAL TRAJECTORIES AND ITS HODOGRAPHIC REPRESENTATION.

THE HODOGRAPHIC REPRESENTATION

Based on the principle of hodographic representation* it is clear that all such Keplerian conics are represented in the dimensionless $\mathcal{X}\mathcal{Y}$ -plane by a unit circle, and the images of all the co-terminal trajectories of a common range angle ψ are given by the same arc of this circle, subtending a central angle ψ between the radii \vec{OQ}_1 and \vec{OQ}_2 which are 90° in advance (in the direction of motion) to the radius vectors \vec{OQ}_1 , \vec{OQ}_2 in the physical plane respectively (Figure 1(b)); the points Q_1 and Q_2 on the circle are therefore the images of the terminal points. To complete the construction of such hodograph one merely needs to locate the origin of the hodograph for each particular trajectory under consideration.

At first sight it seems there might be a wide scattering of such possible origins in the hodograph plane corresponding to the infinitely many possible Keplerian trajectories leading from Q_1 to Q_2 through the same range angle ψ . However, a careful analysis shows that the distribution of such origins is linear. The proof is as follows:

With reference to Figure 2 and the principles given in Ref. 8, the hodograph origin of the trajectory with an arbitrary initial speed parameter λ_1 , and the corresponding final speed parameter λ_2 will lie on both the auxiliary circles (called speed circles) with radii λ_1^2 and λ_2^2 , tangent internally to the unit hodograph circle at Q_1 and Q_2 respectively and therefore at their intersection O_I or O_{II} , the two speed parameters λ_1 and λ_2 being connected by

$$\frac{1-\lambda_2^2}{1-\lambda_1^2} = \frac{r_2}{r_1} \equiv n \quad (2)$$

through the energy integral. Now draw the lines tangent to the hodograph circle at Q_1 and Q_2 respectively, intersecting at T . Then the three lines $O_I O_{II}$, TQ_1 and TQ_2 are the radical axes of the two speed circles and the hodograph circle taken in pairs, therefore, they are concurrent.** That is, the line $O_I O_{II}$ also passes through the point T . Furthermore, from geometry the line $O_I O_{II}$ is perpendicular to the line of centers $G_1 G_2$. But, as shown in Ref. 8 the line $G_1 G_2$ is perpendicular to the chord $Q_1 Q_2$ in the physical plane since the triangles $CG_1 G_2$ (hodograph plane) and $OQ_1 Q_2$ (physical plane) are similar. Consequently $O_I O_{II}$ is parallel to the chord $Q_1 Q_2$. With terminals Q_1 and Q_2 given, T is a fixed point, and the chord $Q_1 Q_2$ is in a fixed direction, thus the line through $O_I O_{II}$ is a fixed straight line, irrespective of the initial speed given by λ_1 . In other words, the intersection of any pair of speed circles, and therefore all the possible hodograph origins will lie

*See Appendix A and Ref. 8 Section V and IX-A, pp. 892-894, 900-904.

**See any standard text on Higher Geometry, e.g. Ref. 2.

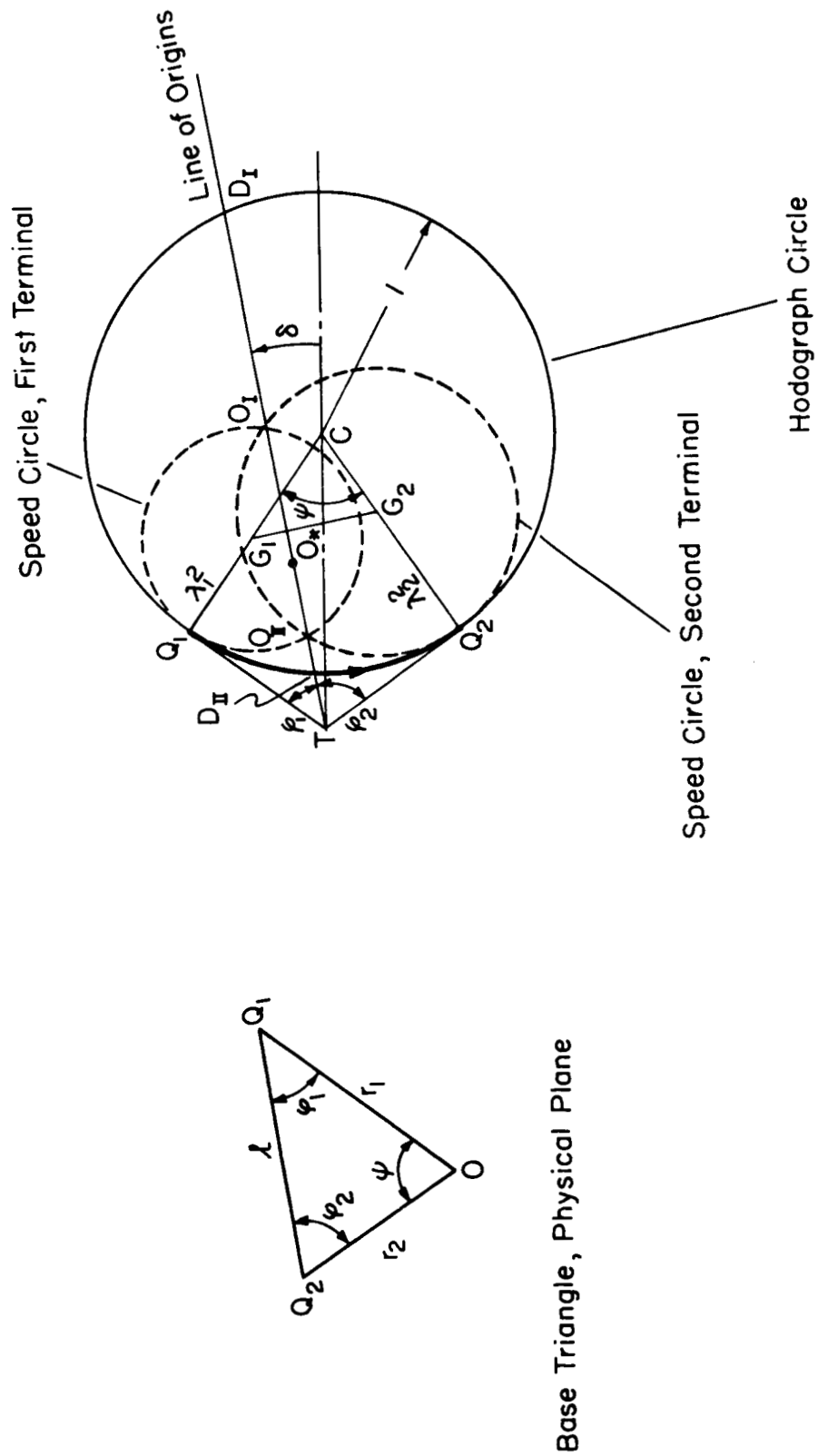


FIGURE 2. PROOF OF THE LINEAR DISTRIBUTION OF THE HODOGRAPH ORIGINS.

on this same line which will be called the line of origins. This completes the proof. It evidently applies to either groups.

Based on the foregoing analysis the hodograph images of all co-terminal trajectories of one group may be represented in the dimensionless hodograph plane by a unit circular arc together with the straight line which passes through the intersection of the tangents to the unit circle at Q_1 and Q_2 , and is parallel to the chord Q_1Q_2 in the physical plane, as shown in Figure 1(b). Each particular point on this line corresponds to a particular trajectory in the physical plane, and the selection of an optimum trajectory to suit some specific purpose is no more than the selection of a certain particular point on this line. Thus in comparison with the complexity of the trajectory geometry in the physical plane the situation in the hodograph plane is far simpler.

It is worth to note that, the hodograph for the complementary group may be obtained by turning that for the normal group through 180° . Thus informations concerning the former may be obtained directly from the hodograph for the latter, and a separate construction for the complementary group is often unnecessary. Besides, as the geometry of the hodograph shows, the angles between the line of origins and the two tangents TQ_1 and TQ_2 are equal to the base angles φ_1 and φ_2 of the base triangle at Q_1 and Q_2 respectively, and the inclination of the line of origins with the centerline CT is given by

$$\delta = \frac{1}{2} (\varphi_2 - \varphi_1) \quad (3)$$

whence $\delta \begin{matrix} > \\ < \end{matrix} 0$ according as $\varphi_1 \begin{matrix} \leq \\ \geq \end{matrix} \varphi_2$ or $r_1 \begin{matrix} > \\ < \end{matrix} r_2$.

A GENERAL SURVEY

Based on the foregoing hodographic representation we may now make a general survey on the nature of the system of the co-terminal Keplerian trajectories associated with an arbitrary base triangle. We will first consider the normal group.

As seen from the hodograph construction, for a given base triangle, there is an initial speed for which the speed circle will tangent to the line of origins. This is the minimum speed below which no such terminal-to-terminal trajectory is possible. The trajectory corresponding to the minimum speed is known as the minimum energy trajectory; its hodograph origin is given by the point of tangency O_* .

When the initial speed exceeds its minimum value, the speed circle will meet the line of origins in two distinct points such as O_I and O_{II} in Figure 2,

giving two distinct trajectories corresponding to the same initial speed. Such trajectories will be referred to as the conjugate trajectories for short, and the corresponding origins, O_I and O_{II} , the conjugate origins. As the hodograph shows, conjugate trajectories have different initial path angles: the one with the low path angle as that associated with O_I is known as the low trajectory; and the one with the high path angle as that associated with O_{II} , the high trajectory. For brevity the corresponding origins will also be called low and high accordingly.

With reference to Figure 2, when the initial speed parameter is less than unity, the origin is within the hodograph circle, and the trajectory is elliptic. As the initial speed increases from its minimum value, the conjugate origins O_I and O_{II} move toward the points D_I and D_{II} respectively. At the points D_I and D_{II} the speed parameter is 1, both trajectories become parabolic. However, it is to be noted that, of this conjugate parabolic pair the high one with its hodograph origin at D_{II} will have its point at infinity (which has D_{II} as its hodograph image) interposed between the terminals Q_1 and Q_2 in the assumed direction of motion, indicating that such a trajectory is physically unrealistic. This is in fact the limiting trajectory which the high elliptic trajectories approach when the initial speed approaches that of escape. As the initial speed further increases, the conjugate origins move from D_I and D_{II} outward respectively, and the trajectories become hyperbolic. On the low trajectory side as the origin moves outward from D_I toward infinity, the eccentricity increases without bound, the trajectory approaches the chord line, and in the limit it degenerates into the chord Q_1Q_2 . This is of course physically impossible since it requires an infinite initial speed. On the high side, as the origin moves outward from D_{II} toward the point T, the eccentricity increases toward CT as its limit, and the two asymptotes of the trajectory hyperbola approach the radii OQ_1 and OQ_2 in the physical plane respectively. However, just like the parabolic case, these high hyperbolic trajectories are unrealistic since their points at infinity are interposed between the terminal points. In the limit when the origin is at T, the trajectory degenerates into the broken line segment Q_2OQ_1 implying again an infinite initial speed, and thus the trajectory is not only unrealistic but also physically impossible. If the origin moves beyond T, the trajectory will be the far branch of a hyperbola which can be realized in a central repulsion field,* but not in a gravity field. These various situations are summarized in Table 1.

Thus in conclusion, for a given base triangle in a Newtonian gravity field the line of origins in the dimensionless hodograph plane starts from the point T and extends toward infinity in the direction of the chord line (Q_1Q_2) in the physical plane; and the origins of all realistic trajectories lie in the open interval from D_I via D_{II} to infinity. Furthermore, the conjugate origins are

*See Ref. 8, Section X, pp. 908-909.

Table 1

Location of the Hodograph Origin and the Nature of the
Terminal--Constrained Trajectory (Range = $\psi < \pi$)

Location of the Hodograph Origin	Type of the Trajectory	Remarks
Between O_* and D_I	elliptic	low trajectory, realistic
Between O_* and D_{II}	elliptic	high trajectory, realistic
At O_*	elliptic	minimum energy, realistic
At D_I	parabolic	low trajectory, realistic
At D_{II}	parabolic	high trajectory, unrealistic
D_I to infinity	hyperbolic	low trajectory, realistic
D_{II} to T	hyperbolic	high trajectory, unrealistic
At infinity	straight line (Q_1Q_2)	infinite speed, physically im- possible
At T	broken line (Q_2OQ_1)	infinite speed, physically im- possible
Beyond T	hyperbolic	realistic in a central repul- sion field, but not in a gravity field

separate by the point O_* with all the low origins situated at the right side of O_* , and all the high origins, its left side (Figure 2); thus the points in the interval O_*D_I and O_*D_{II} are the mutually conjugate elliptic origins; while those in the intervals D_I to infinity, and D_{II} to T are the mutually conjugate hyperbolic origins; and there is one and only one pair of conjugate parabolic origins, the points D_I and D_{II} .

All the foregoing findings for a normal group may be easily adapted to its complement if we note the following:

1. The complement of a high trajectory in one group is a low trajectory in the other;

2. An elliptic trajectory in one group and its complement in the other are both realistic; while the complement of a realistic parabolic or hyperbolic trajectory of one group is unrealistic in the other.

Thus by interchanging the words "high" and "low," and, when a parabolic or a hyperbolic trajectory is concerned, interchanging the words realistic and unrealistic, a similar table for the complementary group may be constructed from Table 1. For the benefit of later development it is also worth to note the following additional relations between a trajectory (realistic or unrealistic) and its complement:

3. All geometrical elements of the two are identical since they are of the same Keplerian conic;

4. All terminal quantities which involve directions are equal in magnitude but opposite in sign, e.g.

$$\vec{V}_1 + \vec{V}'_1 = 0, \quad \phi_1 + \phi'_1 = 0 \quad (4)$$

In the light of the foregoing analysis we see that in the physical plane (Figure 3(a)) the elliptic trajectories of the normal group are all confined in the infinite region (A), while the realistic hyperbolic trajectories of the same group are all confined in the finite region (B). Similarly, elliptic trajectories and the realistic hyperbolic trajectories of the complementary group are all confined in the regions (A') and (B') respectively. The two conjugate parabolas and the three sides of the base triangle form the boundaries of these regions as shown in Figure 3(a). Consequently, the trajectories of both groups associated with a fixed base triangle all lie outside this triangle; and the boundary of this triangle form the limiting trajectories when the speed increases indefinitely.*

LIMITS OF VARIATION OF THE TRAJECTORY ELEMENTS

It is interesting to note that, of the infinitely many Keplerian trajectories associated with a given base triangle there exist certain limits for the possible variations of some of the trajectory elements. As generally known and pointed out earlier, there is a minimum value for the initial terminal speed below which no such trajectory is possible. Consequently there are corresponding limits for the orbital energy, major axis, and the final terminal speed respectively. An examination of the hodograph shows that there exists also a least eccentricity which the trajectory can attain. It is given

*It can be shown that the trajectories will all lie within the base triangle if the field is a central repulsive one.

FIGURE 3. GENERAL SURVEY OF THE SYSTEM OF CO-TERMINAL TRAJECTORIES.

by the perpendicular distance \overline{CE} in Figure 3(d) since the eccentricity is always equal to the origin-to-center distance in the hodograph plane (see Appendix A). Directly from the geometry of the hodograph one finds

$$\epsilon_{\min} = \overline{CE} = \overline{CT} |\sin \delta| = \sec \frac{\psi}{2} \left| \sin \frac{1}{2} (\varphi_2 - \varphi_1) \right| \quad (5)$$

which, after some trigonometric simplifications, reduces to

$$\epsilon_{\min} = \frac{|r_1 - r_2|}{l} = \frac{|1 - n|}{m} \quad (5a)$$

where m is defined by

$$m \equiv \frac{l}{r_1} = \sqrt{1 - 2n \cos \psi + n^2} \quad (6)$$

Thus a circular trajectory is possible only when $r_1 = r_2$ and the greater the numerical difference between the terminal distances, the greater will be the least eccentricity, for a given chord length.

As observed earlier, when the initial speed increases indefinitely the eccentricity of the realistic trajectories of the normal group increases without bound while that of the complementary group approaches \overline{CT} as limit. Thus for such group there is an upper limit for the hyperbolic eccentricity

$$\epsilon_{UL} = \overline{CT} = \sec \frac{\psi}{2} \quad (7)$$

which depends only on the vertex angle of the base triangle, not on the terminal distances. This limiting value itself will approach infinity when ψ approaches π .

Furthermore, the hodograph shows that although the initial speed may increase indefinitely, the corresponding path angle can only vary within two definite limits. For the normal group the upper limit is given by the angle CQ_1D_{II} which the initial path angle of the high elliptic trajectory approaches when the initial speed approaches parabolic. From the hodograph geometry this angle is found to be

$$(\phi_1)_{UL} = \angle CQ_1D_{II} = \frac{1}{2} (\pi + \varphi_1 - \omega) \quad (8)$$

where,

$$\omega = \cos^{-1} \epsilon_{\min} = \cos^{-1} \frac{|1-n|}{m} \quad (9)$$

The lower limit is the path angle for the straight line trajectory Q_1Q_2 which the hyperbolic trajectory approaches. Obviously it is

$$(\phi_1)_{LL} = \varphi_1 - \frac{\pi}{2}. \quad (10)$$

Consequently all possible directions of departure are confined in the angular region (a_1) as shown in Figure 3(b), with an included angle

$$\Delta\phi_1 = (\phi_1)_{UL} - (\phi_1)_{LL} = \pi - \frac{1}{2} (\varphi_1 + \omega) \quad (11)$$

The path angle at the final terminal is likewise limited, and all the possible directions of approach are confined in the angular regions (a_2) in Figure 3(b). Similar regions exist for the complementary group. Consequently, with a given configuration of the base triangle, there are certain forbidden regions for the direction of departure as those marked (b_1) and (c_1) ; and certain forbidden regions for the direction of approach as those marked (b_2) and (c_2) . These limits of variation and the total included angle of each region are listed in Table 2. It is to be noted that, as shown in the table, the regions for possible departure for the normal and the complementary groups have equal included angles, and it can also be verified from the hodograph that they are symmetrically oriented with respect to the bisector of the base angle at the initial terminal; the same is true for the regions of possible approach at the final terminal. Furthermore, the included angle of the inner forbidden region of departure (c_1) and that of the outer forbidden region of approach (b_2) are equal respectively to the base angles at the corresponding terminals; while the included angles of the outer forbidden region of departure (b_1) and the inner forbidden region of approach (c_2) are supplementary to each other. In view of Eq. (5) and Table 2, we may say that for a given vertex angle ψ , the smaller the difference between the base angles, the larger will be the outer forbidden region of departure and the smaller will be the inner forbidden region of approach. In the symmetrical case, $\varphi_1 = \varphi_2$, $r_1 = r_2$, the included angle of the outer forbidden region of departure reaches its maximum and that of the inner forbidden region of approach reaches its minimum, both equal to 90° .

Table 2

Possible and Forbidden Regions of Departure and Approach

	Initial Terminal		Final Terminal	
	Limiting Directions of Departure Formula	Angle in Hodograph	Limiting Directions of Approach Formula	Angle in Hodograph
Normal	$(\phi_1)_{UL} = \frac{1}{2}(\pi + \varphi_1 - \omega)$	$\angle CQ_1D_{II}$	$(\phi_2)_{UL} = \frac{\pi}{2} - \varphi_2$	$\angle CQ_2D_{II}$
	$(\phi_1)_{LL} = \varphi_1 - \frac{\pi}{2}$		$(\phi_2)_{LL} = -\frac{1}{2}(\varphi_2 + \omega)$	
	$(\phi_1')_{UL} = \frac{1}{2}(\pi - \varphi_1 - \omega)$		$(\phi_2')_{UL} = \frac{\pi}{2}$	
	$(\phi_1')_{LL} = -\frac{\pi}{2}$		$(\phi_2')_{LL} = \frac{1}{2}(\varphi_2 - \omega)$	
Complementary		$\angle CQ_1D_I$		$\angle CQ_2D_I$
	Possible Regions of Departure		Possible Regions of Approach	
	Region	Included Angle	Region	Included Angle
Normal	(a_1)	$\Delta\phi_1 = \pi - \frac{1}{2}(\varphi_1 + \omega)$	(a_2)	$\Delta\phi_2 = \frac{1}{2}(\pi - \varphi_2 + \omega)$
	(a_1')	$\Delta\phi_1' = \pi - \frac{1}{2}(\varphi_1 + \omega)$	(a_2')	$\Delta\phi_2' = \frac{1}{2}(\pi - \varphi_2 + \omega)$
Complementary		$\angle Q_1D_{IIT}$		$\angle Q_2D_{IIT}$
	Forbidden Regions of Departure		Forbidden Regions of Entry	
	Region	Included Angle	Region	Included Angle
Inner	(c_1)	φ_1	(c_2)	$\pi - \omega$
	(b_1)	ω	(b_2)	φ_2
Outer		$\angle Q_1TD_{II}$ $\angle ECD_I$		$\angle Q_2TD_{II}$

Finally we observe that the apsidal axes of the present system of trajectories are also confined in certain regions as tabulated below (see also Figure 3(c)).

Table 3
Regions for Apsidal Axes (Positive Portions*)

Trajectories	Boundary Axes	Included Angle
Elliptic	OX_{DI} and OX_{DII}	$\Delta\theta_e = 2\omega$
Hyperbolic Normal Group	OX_{DI} and $OX_{\infty I}$	$\Delta\theta_h = \frac{\pi}{2} - \omega$
Complementary Group	OX_{DII} and $OX_{\infty II}$	$\Delta\theta'_h = \frac{\psi}{2} + \varphi_1 - \omega$

*Defined in Appendix A

Of the four boundary axes, OX_{DI} and OX_{DII} are the apsidal axes of the two parabolic trajectories, while $OX_{\infty I}$ and $OX_{\infty II}$ are those of the limiting hyperbolic trajectories of infinite initial speed. Their directions may be obtained directly from those of the corresponding \mathcal{Y} -axes in the hodograph plane. Evidently, $OX_{\infty I}$ is perpendicular to the chord Q_1Q_2 , and OX_{DII} bisects the vertex angle ψ .

III. THE CHORDAL AND RADIAL COMPONENTS OF THE TERMINAL VELOCITIES

The characteristics of the co-terminal trajectories can be best analyzed by using the chordal and radial components of the terminal velocities. As introduced by Godal in Ref. 5 they are the components in the chordal and radial directions respectively as depicted in Figure 4(a). A method of finding such components in the hodograph will be introduced below.

As shown in Figure 4(b), if O is the origin of the hodograph, then from the proof given in Section II, \overrightarrow{OT} is in the chordal direction, while by construction $\overrightarrow{TQ_1}$ and $\overrightarrow{TQ_2}$ are in the radial directions at Q_1 and Q_2 respectively. Thus in the $\dot{x}\dot{y}$ -plane, that is, if we take the radius of the hodograph circle as μ/h instead of unity, the hodograph gives the terminal velocities

$$\vec{V}_1 = \overrightarrow{OQ_1}, \quad \vec{V}_2 = \overrightarrow{OQ_2} \quad (12)$$

with their chordal and radial components

$$\begin{aligned} \vec{V}_{C1} &= \overrightarrow{OT}, & \vec{V}_{R1} &= \overrightarrow{TQ_1} \\ \vec{V}_{C2} &= \overrightarrow{OT}, & \vec{V}_{R2} &= \overrightarrow{TQ_2} \end{aligned} \quad (13)$$

from which we deduce immediately that

$$\vec{V}_{C1} = \vec{V}_{C2}, \quad V_{R1} = V_{R2} \quad (14)$$

The second relation stems from the fact that the two tangents $\overline{TQ_1}$ and $\overline{TQ_2}$ are equal in length. Thus along the same trajectory the chordal components of the terminal velocities are identical in magnitude and direction, while the radial components are equal in magnitude. Hence if we are dealing with their magnitudes only, the subscripts 1 and 2 are unnecessary and will be dropped hereafter.

Furthermore, the hodograph geometry shows that

$$V_R = \overline{CQ} \tan \frac{\psi}{2} = \frac{\mu}{h} \tan \frac{\psi}{2} \quad (15)$$

With the angular momentum expressed as

$$h = V_C d \quad (16)$$

FIGURE 4. TERMINAL VELOCITIES AND THEIR CHORDAL AND RADIAL COMPONENTS.

where d is the perpendicular distance from the field center to the chord Q_1Q_2 (to be called the base altitude for short), Eq. (15) becomes

$$V_C V_R = \frac{\mu}{d} \tan \frac{\psi}{2} \quad (17)$$

Thus the product of the chordal and radial components of either terminal velocity is constant for all trajectories passing through the given terminal points.

The facts expressed in Eqs. (14) and (17) which were first found by Godal⁵ in his analysis in the physical plane, follow immediately from the present hodograph construction. These simple relations will be useful in the analyses that follow.

IV. CHARACTERISTICS OF THE CONJUGATE TRAJECTORIES

By definition, conjugate trajectories are those having the same initial and final terminal points, same initial speed, and of the same group. (This implies that they have the same range angle.) The proof of the existence of the line of origins has already revealed the existence of a pair of conjugate trajectories for a given base triangle and an arbitrary initial speed ($>V_*$), and lends itself a method of constructing such a conjugate pair in the hodograph plane by simply drawing the speed circle of radius λ_1^2 according to the given speed and finding its intersections with the line of origins, which are then the conjugate origins. With the origins thus determined the elements of each of the conjugate pair may then be found in the usual manner according to the correlation tables in Ref. 8, or Appendix A. The general geometry of such a hodograph is shown in Figure 2; and a typical conjugate pair of each type of the Keplerian trajectories of a normal group and their hodograph images are shown in Figures 5-1, 2, and 3.

Based on such hodographic representation we may now proceed to examine some of the essential features of the conjugate trajectories. With reference to Figure 2 the geometry of the hodograph gives

$$\overline{TO_I} \cdot \overline{TO_{II}} = \overline{TQ_1} \cdot \overline{TQ_2} \quad (18)$$

However, in a dimensionless hodograph we have by definition

$$\begin{aligned} \overline{TO_I} &= \frac{h_I}{\mu} V_{CI}, & \overline{TO_{II}} &= \frac{h_{II}}{\mu} V_{CII} \\ \overline{TQ_1} &= \frac{h_I}{\mu} V_{RI}, & \overline{TQ_2} &= \frac{h_{II}}{\mu} V_{RII} \end{aligned} \quad (19)$$

and furthermore, from the hodograph geometry,

$$\overline{TQ_1} = \overline{TQ_2} = \tan \frac{\psi}{2} \quad (20)$$

Substituting Eqs. (19) and (20) into (18) and making use of Eq. (16) yields

$$V_{CI} \cdot V_{CII} = V_{RI} \cdot V_{RII} = \frac{\mu}{d} \tan \frac{\psi}{2} \quad (21)$$

Thus for fixed terminal points the product of the conjugate chordal components of the terminal velocity and that of the conjugate radial components are identical, both equal to the same constant, determined by the geometry of the base triangle.

Furthermore, combining Eqs. (21) and (17) gives the reciprocal relations,

$$V_{CI} = V_{RII}, \quad V_{RI} = V_{CII} \quad (22)$$

That is, by merely interchanging the chordal and radial components of the velocity at either terminal we may change the trajectory to its conjugate.

Next, since the angular momentum is directly proportional to the terminal chordal component, it follows immediately from Eqs. (21) and (16) that the conjugate angular momenta are related by

$$h_I \cdot h_{II} = \mu d \tan \frac{\psi}{2} \quad (23)$$

Furthermore, as the latus rectum of the trajectory conic is determined by the angular momentum according to

$$\bar{r} = \frac{h^2}{\mu} \quad (24)$$

Eq. (23) leads to

$$\bar{r}_I \cdot \bar{r}_{II} = d^2 \tan^2 \frac{\psi}{2} \quad (25)$$

The above equations show that in a given gravity field the product of each pair of the conjugate elements, V_C , V_R , h , and \bar{r} , is a constant, depending on the geometry of the base triangle, but independent of the initial speed, and hence the choice of trajectory. In the case of the product of latus recta it is also independent of the field strength μ . Furthermore, as these products involve no other geometrical parameters than ψ and d , base triangles of different configurations will have the same values of these conjugate products as long as they have the same vertex angle and the same base altitude.

Finally as shown in Figures 5 the hodograph gives the conjugate path angles at the initial terminal Q_1 for either type of the trajectory,

$$\phi_{1I} = \angle CQ_1O_I, \quad \phi_{1II} = \angle CQ_1O_{II} \quad (26)$$

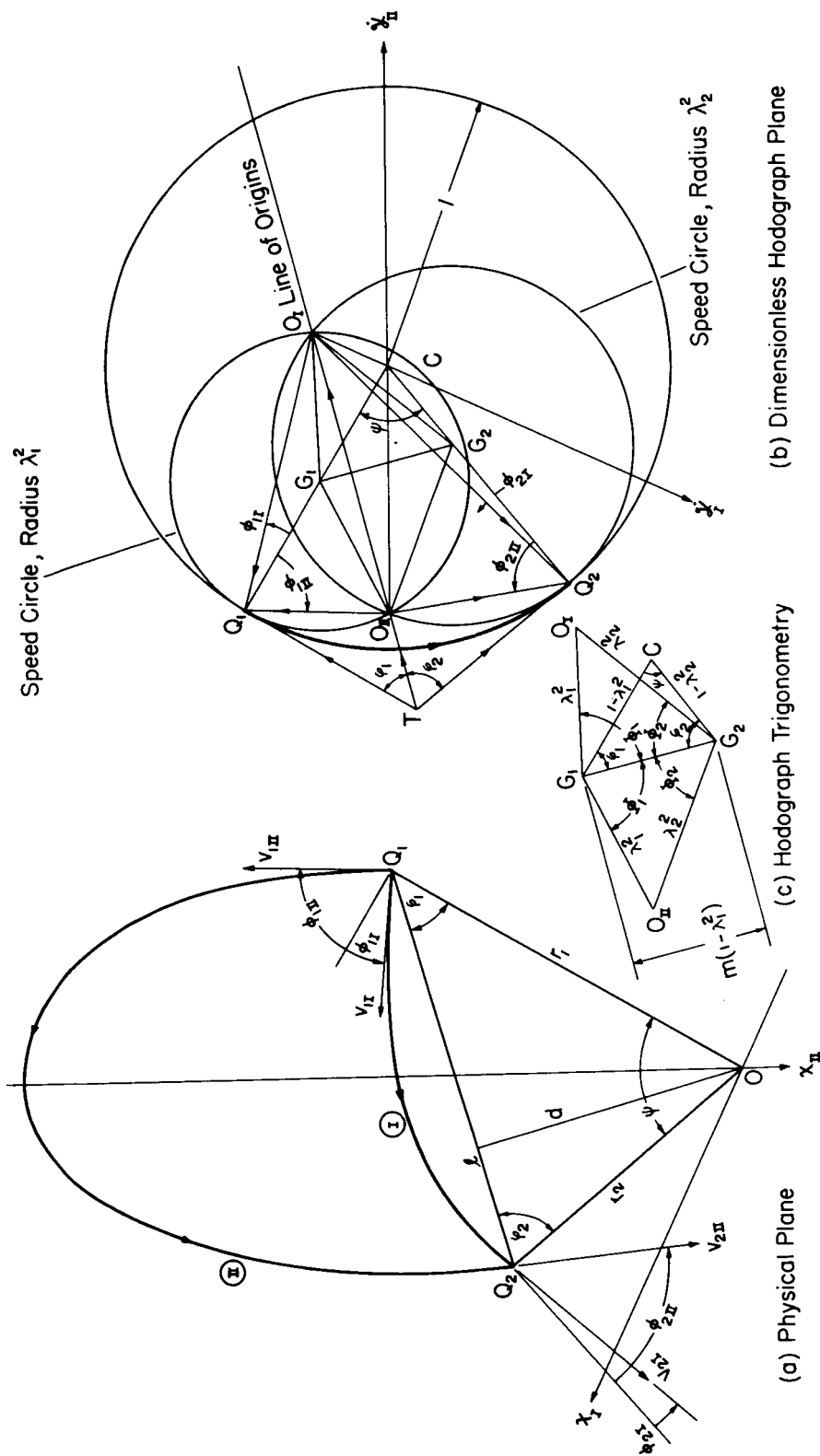


FIGURE 5-1. THE CONJUGATE ELLIPTIC TRAJECTORIES,
RANGE $< 180^\circ$.

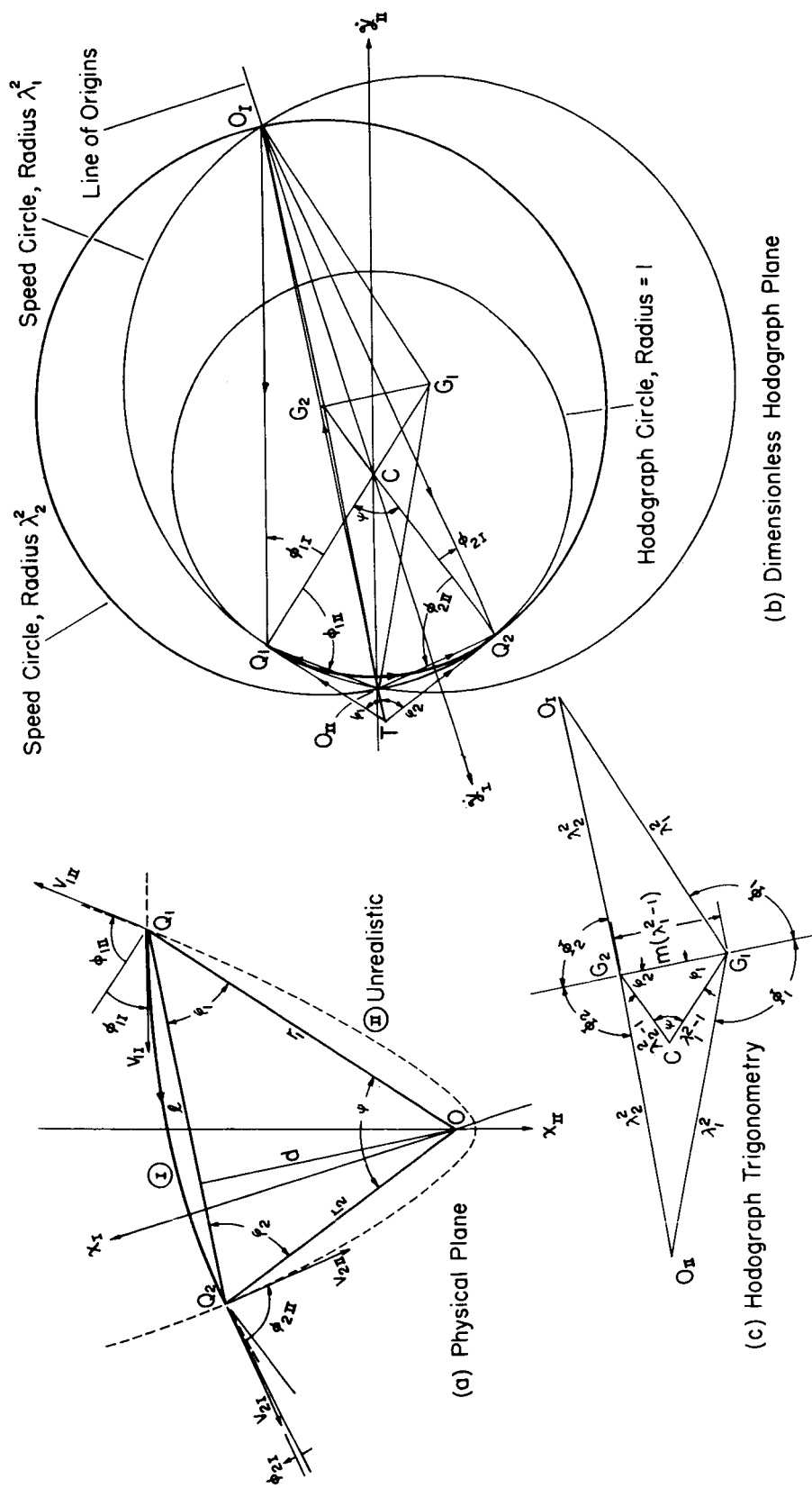


FIGURE 5-2. THE CONJUGATE HYPERBOLIC TRAJECTORIES,
RANGE $< 180^\circ$.

FIGURE 5-3. THE CONJUGATE PARABOLIC TRAJECTORIES, RANGE $< 180^\circ$.

Based on the sign convention for the angular measurement of ϕ and the geometry of the hodograph (Figure 5-1) it is seen that, for an elliptic trajectory,

$$\angle CQ_1O_I = \frac{1}{2} (\angle CG_1G_2 - \angle O_I G_1 G_2)$$

$$\angle CQ_1O_{II} = \frac{1}{2} (\angle CG_1G_2 + \angle O_{II} G_1 G_2)$$

By the similarity of the triangles CG_1G_2 in the hodograph plane and OQ_1Q_2 in the physical plane, the angle CG_1G_2 may be identified as the base angle ϕ_1 ; and by hodograph construction the angles $O_I G_1 G_2$ and $O_{II} G_1 G_2$ are equal in magnitude, denoted by Φ_1 . Thus the foregoing relations may be written as

$$\phi_{1I} = \frac{1}{2} (\phi_1 - \Phi_1) \quad (27)$$

$$\phi_{1II} = \frac{1}{2} (\phi_1 + \Phi_1)$$

from which we deduce immediately

$$\phi_{1I} + \phi_{1II} = \phi_1 \quad (28-1)$$

Evidently, similar relation holds at the final terminal Q_2 , that is

$$\phi_{2I} + \phi_{2II} = \phi_2 \quad (28-2)$$

An examination of the hodograph geometry for the hyperbolic case (Figure 5-2) shows that Eq. (27) also holds if we define Φ_1 to be $\pi - \angle O_I G_1 G_2$. Both definitions for Φ_1 become identical for the parabolic case (Figure 5-3) in which the points G_1 and G_2 coincide at C_1 (the center of the hodograph circle), and the limiting direction of G_1G_2 is given by the line through C and perpendicular to the line of origins. Consequently Eqs. (28) are also valid for the hyperbolic and parabolic cases. Thus in conclusion, the algebraic sum of the conjugate path angles at either terminal is equal to the vertex angle of the base triangle at that terminal. Since for fixed terminal points, ϕ_1 and ϕ_2 are constants, we may say that the algebraic sum of the conjugate path angles at either terminal is constant, independent of the initial speed, hence the choice of trajectory. This conclusion has been previously established in the author's earlier work⁷ for the symmetric, elliptic case, the present analysis shows that it carries over to the general case not necessarily symmetric, and covering all three types of the Keplerian trajectories even though the high trajectory is not realistic in the hyperbolic or parabolic case.

In addition to the conjugate relations deduced so far, it is well known that the conjugate trajectories, being of the same initial speed always have the same orbital energy, same magnitude of the major-axis, and the same speed at the final terminal, that is

$$k_I = k_{II}, \quad a_I = a_{II}, \quad V_{2I} = V_{2II} \quad (29)$$

Eqs. (21) to (23), (25), (28) and (29) constitute the essential relations between the conjugate trajectories.

With the previous understanding outlined in Section II all conjugate relations in this section developed for a normal group hold for its complement except proper changes of signs are needed in the formulas involving path angles according to Eq. (4).

V. THE PRINCIPAL ELEMENTS OF THE CONJUGATE TRAJECTORIES

In ballistic missile problems or problems of interplanetary flight it is usually desirable to determine the trajectory elements for an arbitrary initial speed V_1 when the range angle ψ and the terminal distances r_1 and r_2 are prescribed, that is when the base triangle is given. The hodograph construction described in Section III has already provided a simple graphical means for the determination of such elements. If analytical expressions are sought, we may easily proceed from the geometry of the hodograph.

A simple way for such derivation is again to start from the chordal and radial components of the terminal velocity. Let us first consider the trajectories of the normal group. As the hodograph shows (Figure 4), for a given initial speed V_1 these two components are related by

$$V_C^2 + V_R^2 = V_1^2 + 2V_C V_R \cos \varphi_1 \quad (30)$$

Combining it with the constant product relation (17) yields the pair of solutions

$$V_C = \frac{1}{2} \left[\sqrt{V_1^2 + \frac{4\mu}{d} \tan \frac{\psi}{2} \cos^2 \frac{\varphi_1}{2}} \pm \sqrt{V_1^2 - \frac{4\mu}{d} \tan \frac{\psi}{2} \sin^2 \frac{\varphi_1}{2}} \right] \quad (31-1)$$

$$V_R = \frac{1}{2} \left[\sqrt{V_1^2 + \frac{4\mu}{d} \tan \frac{\psi}{2} \cos^2 \frac{\varphi_1}{2}} \pm \sqrt{V_1^2 - \frac{4\mu}{d} \tan \frac{\psi}{2} \sin^2 \frac{\varphi_1}{2}} \right] \quad (31-2)$$

where the upper sign corresponds to the high trajectory of the conjugate pair and the lower sign, the low trajectory. (This double-sign convention will be followed through in all the later development.)

With these formulas as basis, other trajectory elements follow immediately from the general orbital relations. For convenience we set

$$\zeta = \sqrt{V_1^2 + \frac{4\mu}{d} \tan \frac{\psi}{2} \cos^2 \frac{\varphi_1}{2}} \quad (32)$$

$$\chi = \sqrt{V_1^2 - \frac{4\mu}{d} \tan \frac{\psi}{2} \sin^2 \frac{\varphi_1}{2}}$$

and write

$$v_C = \frac{1}{2} (\xi \bar{r} \chi) \quad (33)$$

It then follows that

$$h = v_C d = \frac{d}{2} (\xi \bar{r} \chi) \quad (34)$$

$$v_{\theta 1} = \frac{h}{r_1} = \frac{d}{2r_1} (\xi \bar{r} \chi) \quad (35)$$

$$\cos \phi_1 = \frac{v_{\theta 1}}{v_1} = \frac{d}{2r_1 v_1} (\xi \bar{r} \chi) \quad (36)$$

$$\frac{\bar{r}}{r} = \frac{h^2}{\mu} = \frac{d^2}{4\mu} (\xi \bar{r} \chi)^2 \quad (37)$$

$$\epsilon = \left[1 - 2(1 - \lambda_1^2) \frac{\bar{r}}{r_1} \right]^{1/2} = \left[1 - \frac{d^2}{2\mu r_1} (1 - \lambda_1^2) (\xi \bar{r} \chi)^2 \right]^{1/2} \quad (38)$$

and so on. By using the trigonometric relations among the geometrical elements of the base triangle, the trajectory elements given by the foregoing formulas may all be expressed in terms of the three independent elements of the base triangle, ψ , ϕ_1 , and r_1 , together with the initial speed. The results are summarized in column 1, Table 4. For convenience, all speeds have been expressed in the dimensionless form of speed parameters. The transition from the present set of independent variables to the more usual combination: ψ , n , r_1 , and λ_1 is straightforward though tedious. To avoid long, cumbersome expressions, a redundant variable m defined by Eq. (6) is introduced, and the results are given in column 2, Table 4.

It is to be noted that, since Eqs. (17) and (30) on which the present derivation is based, are independent of the type of the trajectory, so are all the formulas shown in Table 4. Finally in line with the observations in Section II although the formulas here stand for all three types of the Keplerian trajectory, they may or may not be realistic (see footnote, Table 4).

Table 4

Formulae for the Principal Elements of the Conjugate Trajectories

	Range Angle = $\psi < \pi$	
	In terms of ψ, q, λ, n and λ_1	In terms of ψ, m, n, λ_1 and λ
Initial Terminal Speed Parameter		
Chordal λ_c	$\frac{1}{2} \left[\sqrt{\lambda^2 + \tan^2 \frac{\psi}{2} \cot^2 \frac{\psi}{2}} \pm \sqrt{\lambda^2 - \tan^2 \frac{\psi}{2} \tan^2 \frac{\psi}{2}} \right]$	$\frac{1}{2} \left[\sqrt{\lambda^2 + \frac{m-n \cos \psi}{2n} \sec^2 \frac{\psi}{2}} \pm \sqrt{\lambda^2 - \frac{m-n \cos \psi}{2n} \sec^2 \frac{\psi}{2}} \right]$
Radial λ_r	$\pm \left[\sqrt{\lambda^2 + \tan^2 \frac{\psi}{2} \cot^2 \frac{\psi}{2}} \pm \sqrt{\lambda^2 - \tan^2 \frac{\psi}{2} \tan^2 \frac{\psi}{2}} \right]$	$\pm \left[\sqrt{\lambda^2 + \frac{m-n \cos \psi}{2n} \sec^2 \frac{\psi}{2}} \pm \sqrt{\lambda^2 - \frac{m-n \cos \psi}{2n} \sec^2 \frac{\psi}{2}} \right]$
Transverse λ_{tr}	$\sin^2 \frac{\psi}{2} \left[\sqrt{\lambda^2 + \tan^2 \frac{\psi}{2} \cot^2 \frac{\psi}{2}} \pm \sqrt{\lambda^2 - \tan^2 \frac{\psi}{2} \tan^2 \frac{\psi}{2}} \right]$	$\frac{1}{2} \frac{n}{m} \sin^2 \psi \left[\sqrt{\lambda^2 + \frac{m-n \cos \psi}{2n} \sec^2 \frac{\psi}{2}} \pm \sqrt{\lambda^2 - \frac{m-n \cos \psi}{2n} \sec^2 \frac{\psi}{2}} \right]$
Radial λ_r	$\sin^2 \frac{\psi}{2} \left[\sqrt{\lambda^2 + \tan^2 \frac{\psi}{2} \cot^2 \frac{\psi}{2}} \pm \cos^2 \frac{\psi}{2} \sqrt{\lambda^2 - \tan^2 \frac{\psi}{2} \tan^2 \frac{\psi}{2}} \right]$	$\left[\frac{m+n \cos \psi}{2m} - \sqrt{\lambda^2 + \frac{m-n \cos \psi}{2n} \sec^2 \frac{\psi}{2}} \pm \frac{m-n \cos \psi}{2m} \pm \frac{m-n \cos \psi}{2n} \sqrt{\lambda^2 - \frac{m-n \cos \psi}{2n} \sec^2 \frac{\psi}{2}} \right]$
Initial Path Angle ϕ_i	$\frac{1}{2} \left[\phi_1 \pm \cos^{-1} \left(\frac{1}{\lambda^2} \tan^2 \frac{\psi}{2} \sin^2 \frac{\psi}{2} - \cos \phi_1 \right) \right]$ $= \cos^{-1} \left\{ \frac{\sin \phi_1}{2 \lambda^2} \left[\sqrt{\lambda^2 + \tan^2 \frac{\psi}{2} \cot^2 \frac{\psi}{2}} \pm \sqrt{\lambda^2 - \tan^2 \frac{\psi}{2} \tan^2 \frac{\psi}{2}} \right] \right\}$	$\frac{1}{2} \left[\cos^{-1} \frac{1-n \cos \psi}{m} \pm \cos^{-1} \frac{1-n \cos \psi}{m \lambda^2} \right]$ $= \cos^{-1} \left\{ \frac{1}{2} \left(\frac{n}{m} \right) \sin^2 \psi \left[\sqrt{\lambda^2 + \frac{m-n \cos \psi}{2n} \sec^2 \frac{\psi}{2}} \pm \sqrt{\lambda^2 - \frac{m-n \cos \psi}{2n} \sec^2 \frac{\psi}{2}} \right] \right\}$
Angular Momentum h	$\sqrt{\lambda^2} \sin^2 \frac{\psi}{2} \left[\sqrt{\lambda^2 + \tan^2 \frac{\psi}{2} \cot^2 \frac{\psi}{2}} \pm \sqrt{\lambda^2 - \tan^2 \frac{\psi}{2} \tan^2 \frac{\psi}{2}} \right]$	$\sqrt{\lambda^2} \frac{n}{m} \sin^2 \psi \left[\sqrt{\lambda^2 + \frac{m-n \cos \psi}{2n} \sec^2 \frac{\psi}{2}} \pm \sqrt{\lambda^2 - \frac{m-n \cos \psi}{2n} \sec^2 \frac{\psi}{2}} \right]$
Orbital Energy k	$\frac{h_c}{\lambda^2} (\lambda^2 - 1)$	$\frac{h_c}{\lambda^2} (\lambda^2 - 1)$
Semi-major Axis q (or Semi-transverse Axis)	$\frac{\lambda_1}{2 1 - \lambda^2 }$	$\frac{\lambda_1}{2 1 - \lambda^2 }$
Semi-latus Rectum \bar{r}	$\lambda_1 \sin^2 \psi \left[\lambda^2 + \tan^2 \frac{\psi}{2} \cot^2 \frac{\psi}{2} \pm \sqrt{\lambda^2 + \tan^2 \frac{\psi}{2} \cot^2 \frac{\psi}{2}} - \tan^2 \frac{\psi}{2} \right]$	$\lambda_1 \left(\frac{n}{m} \right)^2 \sin^2 \psi \left[\lambda^2 + \frac{1-n \cos \psi}{2n} \sec^2 \frac{\psi}{2} \pm \sqrt{\lambda^2 + \frac{1-n \cos \psi}{2n} \sec^2 \frac{\psi}{2}} - \tan^2 \frac{\psi}{2} \right]$
Eccentricity e	$\left\{ 1 - 2(1 - \lambda^2) \sin^2 \phi_1 \left[\lambda^2 + \tan^2 \frac{\psi}{2} \cot^2 \frac{\psi}{2} \pm \sqrt{\lambda^2 + \tan^2 \frac{\psi}{2} \cot^2 \frac{\psi}{2}} - \tan^2 \frac{\psi}{2} \right] \right\}^{\frac{1}{2}}$	$\left\{ 1 - 2(1 - \lambda^2) \left(\frac{n}{m} \right)^2 \sin^2 \psi \left[\lambda^2 + \frac{1-n \cos \psi}{2n} \sec^2 \frac{\psi}{2} \pm \sqrt{\lambda^2 + \frac{1-n \cos \psi}{2n} \sec^2 \frac{\psi}{2}} - \tan^2 \frac{\psi}{2} \right] \right\}^{\frac{1}{2}}$
Definitions:	$n \equiv \frac{\lambda_1}{\lambda^2} \quad m \equiv \frac{\lambda_1}{\lambda^2} = \sqrt{1 - 2m \cos \psi + m^2}$	

Note: 1. All formulas hold for all three types of the Keplerian trajectories, elliptic, parabolic, and hyperbolic.
 2. Of the double sign, the upper one refers to the high trajectory, while the lower one, the lower trajectory.
 3. Quantities pertaining to the final terminal may be obtained from the corresponding formula for the initial terminal by replacing the subscript "1" by "2", and n by $1/n$ (m by m/n).
 4. To obtain formulas for range angle $\psi' = 2\pi - \psi > \pi$, interchange the upper and lower sign and replace ϕ_1 by $-\phi_1$.

Among these principal elements of the conjugate trajectories the initial path angle ϕ_1 deserves particular attention since it determines the correct direction of departure for an arbitrary initial speed. However, formula (36) may result in some ambiguity in finding the angle ϕ_1 from its cosine since ϕ_1 may be either positive or negative. An alternative formula may be obtained by directly resorting to Eqs. (27). Observing the triangles OQ_1Q_2 (physical plane) and $O G_1G_2$ (hodograph plane) in Figure 5-1 or 5-2 and applying the cosine law we find

$$\cos \varphi_1 = \frac{1-n \cos \psi}{m} \quad (39)$$

$$\cos \phi_1 = \frac{n-1 + (1-n \cos \psi)(1-\lambda_1^2)}{m \lambda_1^2} = \frac{1}{\lambda_1^2} \tan \frac{\psi}{2} \sin \varphi_1 - \cos \varphi_1 \quad (40)$$

Inserting these expressions into Eqs. (26) we obtain

$$\phi_1 = \frac{1}{2} \left[\cos^{-1} \frac{1-n \cos \psi}{m} \pm \cos^{-1} \frac{n-1 + (1-n \cos \psi)(1-\lambda_1^2)}{m \lambda_1^2} \right] \quad (41-a)$$

$$= \frac{1}{2} \left[\varphi_1 \pm \cos^{-1} \left(\frac{1}{\lambda_1^2} \tan \frac{\psi}{2} \sin \varphi_1 - \cos \varphi_1 \right) \right] \quad (41-b)$$

Under the assumption $0 < \psi < \pi$ we have $0 < \varphi_1 < \pi$, and $0 < \phi < \pi$. Consequently both equations here give a unique value of ϕ_1 for each of the conjugate pair without ambiguity. Note here that Eq. (39) is a purely trigonometric relation of the base triangle, while with the angle ϕ defined in Figures 5-1, 2, and 3 for the elliptic, hyperbolic and parabolic cases respectively, Eq. (40) applies to all three types of trajectories. Thus, just like Eq. (26) the present expressions (41-a, b) hold regardless of the type of the trajectory even though it may not be realistic.

Evidently all formulas of this section may apply to the complementary group with a change of sign for the path angle and interchange of the upper and lower signs in the double-sign convention. The dependence of the path angle and the trajectory eccentricity on the range angle, the distance ratio, and the initial speed are shown graphically in Figures 11-1 and 2.

Very often the maximum and minimum radial distances on the trajectory are of interest. One should be aware of the fact that, since the trajectory is only a part of the Keplerian conic, the two apses may or may not lie on the trajectory, and consequently the maximum and minimum radial distances may or

may not be given by the apocenter and pericenter distances as usually calculated from

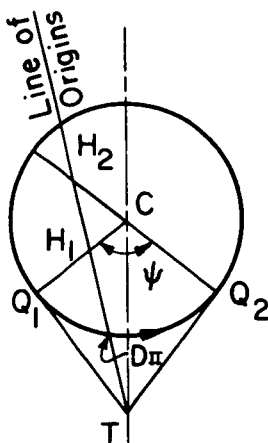
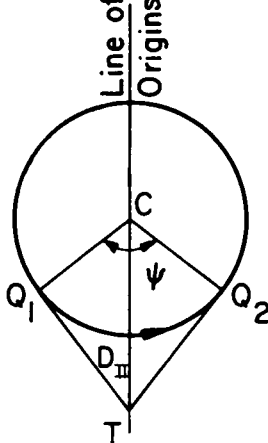
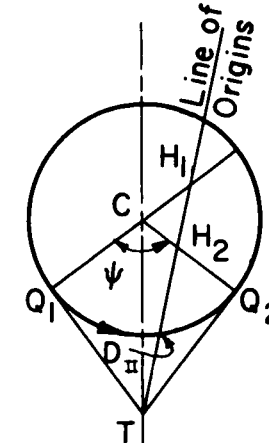
$$r_A = a(1+\epsilon), \quad r_P = a|1-\epsilon| \quad (42)$$

In the hodograph plane this is indicated by whether or not the \dot{y} -axis (the line through O and C) will cross the arc Q_1Q_2 , the hodograph image of the trajectory; and this is in turn determined by the location of the hodograph origin relative to the two key points H_1 and H_2 , the intersections of the line of origins with the radii OQ_1 and OQ_2 (or their extensions) respectively. An examination of the hodograph will help to clarify the situation and the criteria obtained are summarized in Table 5. Thus in a normal group it is possible to have either the apocenter or the pericenter alone, or none of them, but never both lying on the trajectory. In case the apocenter or the pericenter does not lie on the trajectory, then the maximum or minimum distances, instead of being given by Eqs. (42) will be either r_1 or r_2 itself. It is to be noted that same criteria of Table 5 may apply to a complementary group if we interchange the letters A and P.

Finally, the duration of terminal-to-terminal flight is usually of importance in determining the actual range of a ballistic missile over a rotating planet, and in many problems of orbital transfer or interplanetary flight. Various expressions are available for such calculations; however, with fixed terminal points the most convenient way is to apply Lambert's theorem.¹ In the present case one needs to note whether the segment formed by a realistic trajectory and the chord Q_1Q_2 contains both foci, the attracting focus alone, the vacant focus alone, or none of them (the vacant focus of parabola being considered at infinity). The results of such application are summarized in Appendix B and the dependence of the time of flight on the range angle, terminal distances and the initial speed are shown graphically in Figures 11-3(a),(b) and (c).

Table 5

Hodographic Criteria for the Occurrence of the Apses on the Trajectory ($\psi < \pi$)

	(a) $n < 1$	(b) $n = 1$	(c) $n > 1$
			
Occurrence of Apsis on the Trajectory	Location of the Hodograph Origin		
	$n < 1$	$n = 1$	$n > 1$
A, not P	Between D_{II} and H_1	Between D_{II} and C	Between D_{II} and H_2
P, not A	Beyond H_2	Beyond C	Beyond H_1
Neither A nor P	Between H_1 and H_2	---	Between H_1 and H_2

VI. ANALYSIS OF SOME PARTICULAR TRAJECTORIES

The trajectory analysis made so far has been of a general nature, a brief analysis for some of the particular trajectories is now in order.

THE MINIMUM ENERGY TRAJECTORY

Since the minimum energy trajectory is fairly well-known,* only a few supplementary remarks will be sufficient.

In line with the concept of conjugate trajectories a minimum energy trajectory may be viewed as the one conjugate to itself. By using this concept all formulas for the minimum energy trajectory follow immediately from those for the conjugate trajectories. For example, setting $V_{CI} = V_{CII} = V_{C*}$, $V_{RI} = V_{RII} = V_{R*}$ in (21) we find

$$V_{C*} = V_{R*} = (V_{CI}V_{CII})^{1/2} = (V_{RI}V_{RII})^{1/2} = \left(\frac{\mu}{d} \tan \frac{\psi}{2}\right)^{1/2} \quad (43)$$

Thus the minimum energy trajectory is characterized by the fact that the chordal and radial components of either terminal velocity are identical in magnitude, both equal to the geometrical mean of any conjugate pair of either the chordal components or the radial components, with the same ψ and d . Formula (43) is in fact self-evident from the geometry of the hodograph since in the present case (see Figure 6) the speed circle at Q_1 is tangent to both the line of origin and the line TQ_1 and the two tangents drawn from an exterior point to a circle are necessarily equal. This simple fact enables one to locate the optimum origin O_* in the hodograph plane for the minimum energy trajectory by simply laying off $TO_* = TQ_1$ on the line of origins.

Likewise by using the same concept we deduce

$$h_* = (h_I h_{II})^{1/2} = \left(\mu d \tan \frac{\psi}{2}\right)^{1/2} \quad (44)$$

$$\bar{r}_* = (\bar{r}_1 \bar{r}_2)^{1/2} = d \tan \frac{\psi}{2} \quad (45)$$

*See for example Ref. 4, 7, 8, 9.

FIGURE 6. THE MINIMUM ENERGY TRAJECTORY AND ITS RELATION WITH A PAIR OF CONJUGATE TRAJECTORIES, RANGE $< 180^\circ$.

$$\phi_{1*} = \frac{1}{2} (\phi_{1I} + \phi_{1II}) = \frac{1}{2} \varphi_1 \quad (46-1)$$

$$\phi_{2*} = \frac{1}{2} (\phi_{2I} + \phi_{2II}) = \frac{1}{2} \varphi_2 \quad (46-2)$$

Thus the optimum values of the angular momentum and latus rectum for minimum energy trajectory are the geometrical means of any conjugate pairs of the angular momenta and latus recta respectively for the same range angle ψ and the base altitude d ; while the optimum terminal path angle is the arithmetic mean of any conjugate pair of the terminal path angles for the same base angle at the terminal point, and is equal to one half of this base angle. The last statement on the path angle, in fact, amounts to saying: the optimum direction of departure for a minimum energy trajectory always bisects a pair of conjugate directions of departure and the same is true for the resulting direction of approach. This conclusion has been previously established in Ref. 7 for the symmetrical case. The present analysis shows that it carries over to the unsymmetrical case just as well. In particular, the optimum direction bisects the external angle at the corresponding terminal since the chordal and radial directions at either terminal are such a conjugate pair; thus the optimum direction and the bisector of the base angle at the same terminal are perpendicular to each other. It is interesting to note here that the direction of optimum departure is determined by the initial base angle alone. Consequently this direction will remain fixed if the final terminal moves along the chord line. This is in analogy with an artillery trajectory over a flat earth. Imagine a target point is in the same horizontal plane as the initial point, then $\phi_1 = 90^\circ$, and Eq. (46-1) gives the optimum direction of departure at 45° with the local horizon just like the artillery case, although the force field considered here is central instead of uniform. The only main difference is that the trajectory here is elliptic instead of parabolic.

The optimum initial speed parameter for the minimum energy trajectory is given by the hodograph as the radius of the speed circle at Q_1 which is tangent to the line of origins, and the geometry of the hodograph (Figure 6) shows that

$$\lambda_{1*}^2 = \tan \frac{\psi}{2} \tan \frac{\phi_1}{2} \quad (47)$$

which, after some trigonometric simplifications, reduces to the formula given in Ref. 8,

$$\lambda_{1*}^2 = 1 - \frac{r_1}{s} \quad (47-a)$$

where s is the half-perimeter of the base triangle, defined by

$$s = \frac{1}{2} (r_1 + r_2 + l) \quad (48)$$

The minimum energy and the corresponding semimajor axis are then found to be

$$k_* = \frac{\mu}{r_1} (\lambda_{1*}^2 - 1) = -\frac{\mu}{s} \quad (49)$$

and

$$a_* = \frac{r_1}{2(1 - \lambda_{1*}^2)} = \frac{1}{2} s \quad (50)$$

Thus, in a given field, while the angular momentum and the latus rectum of a minimum energy trajectory are determined by ψ and d alone the orbital energy and the major axis depend only on the perimeter of the base triangle.

Following the foregoing formulas all other elements of a minimum energy trajectory may be easily obtained from the general orbital relations. Of course all formulas and conclusions in this section hold for a normal group or its complement as well except for a change of sign in the path angle, since the minimum energy trajectories of the two groups are of the same Keplerian ellipse.

In regard to the occurrence of the apses, it is to be noted that, for a normal group the apocenter of a minimum energy trajectory always lies on the trajectory while its pericenter does not, since the optimum origin O_* in such case always lies between the points H_1 (or H_2) and D_{II} (see Table 5). Thus for such trajectory the apocenter is actually the trajectory peak while the point of closest approach on the trajectory is either Q_1 or Q_2 according as $r_1 < r_2$, or $r_1 > r_2$. A similar statement holds for a complementary group except that it is the pericenter which always lies on the trajectory, not the apocenter. Sometimes the location of such apses on the trajectory is of interest. By considering the similarities of the triangles OQ_1Q_2 (physical plane) and CG_1G_2 (hodograph plane) a little trigonometric manipulation yields

$$\begin{aligned} \tan \psi_1 &= \frac{\sin \psi}{\cos \psi + \kappa} \\ \tan \psi_2 &= \frac{\sin \psi}{\cos \psi + \frac{1}{\kappa}} \end{aligned} \quad (51)$$

where the angles ψ_1 and ψ_2 are identified in Figure 6, and

$$\kappa = \left(\sin \frac{\phi_1}{2} / \sin \frac{\phi_2}{2} \right)^2 \quad (52)$$

which is a constant for a given base triangle. The above equations give the location of the apocenter for a normal minimum energy trajectory or the pericenter of its complement.

THE LEAST ECCENTRIC TRAJECTORY AND ITS CONJUGATE

As shown in Section II, there is a least eccentric trajectory for each fixed configuration of the base triangle. The hodograph origin for such trajectory is given by the point E, the foot of the perpendicular drawn from the center of the hodograph circle to the line of origins, and the least eccentricity is given by Eq. (5) or (5a). The dependence of ϵ_{\min} on n and ψ is shown graphically in Figures 11-2-a,b,c,d as the least eccentricity line which forms the lower envelope for all the eccentricity curves. Obviously with its hodograph origin located at E, a least eccentric trajectory will have its apsidal axis parallel to the chord line Q_1Q_2 in the physical plane, and consequently its minor axis will pass through the middle point of the chord Q_1Q_2 (Figure 7).

It can be shown that the trajectory conjugate to the least eccentric one is the one having its hodograph origin located at F, where the line of origins crosses the line Q_1Q_2 in the hodograph plane. This trajectory ellipse will have the line Q_1Q_2 as its diameter since the terminal velocities are now pointing in the opposite directions. The initial path angle to achieve this particular trajectory of a normal group is, as seen from the hodograph,

$$\phi_{1II} = -\phi_{2II} = \frac{\pi}{2} - \frac{\psi}{2} \quad (53-II)$$

The conjugate path angle, which is the one to achieve the least eccentric trajectory is then, according to Eq. (28-1)

$$\phi_{1I} = -\phi_{1II} = \frac{1}{2} (\phi_1 - \phi_2) \quad (53-I)$$

The initial speed ratio λ_1 required for both trajectories and the resulting final speed ratio λ_2 may be easily found by noting that the speed ratios at

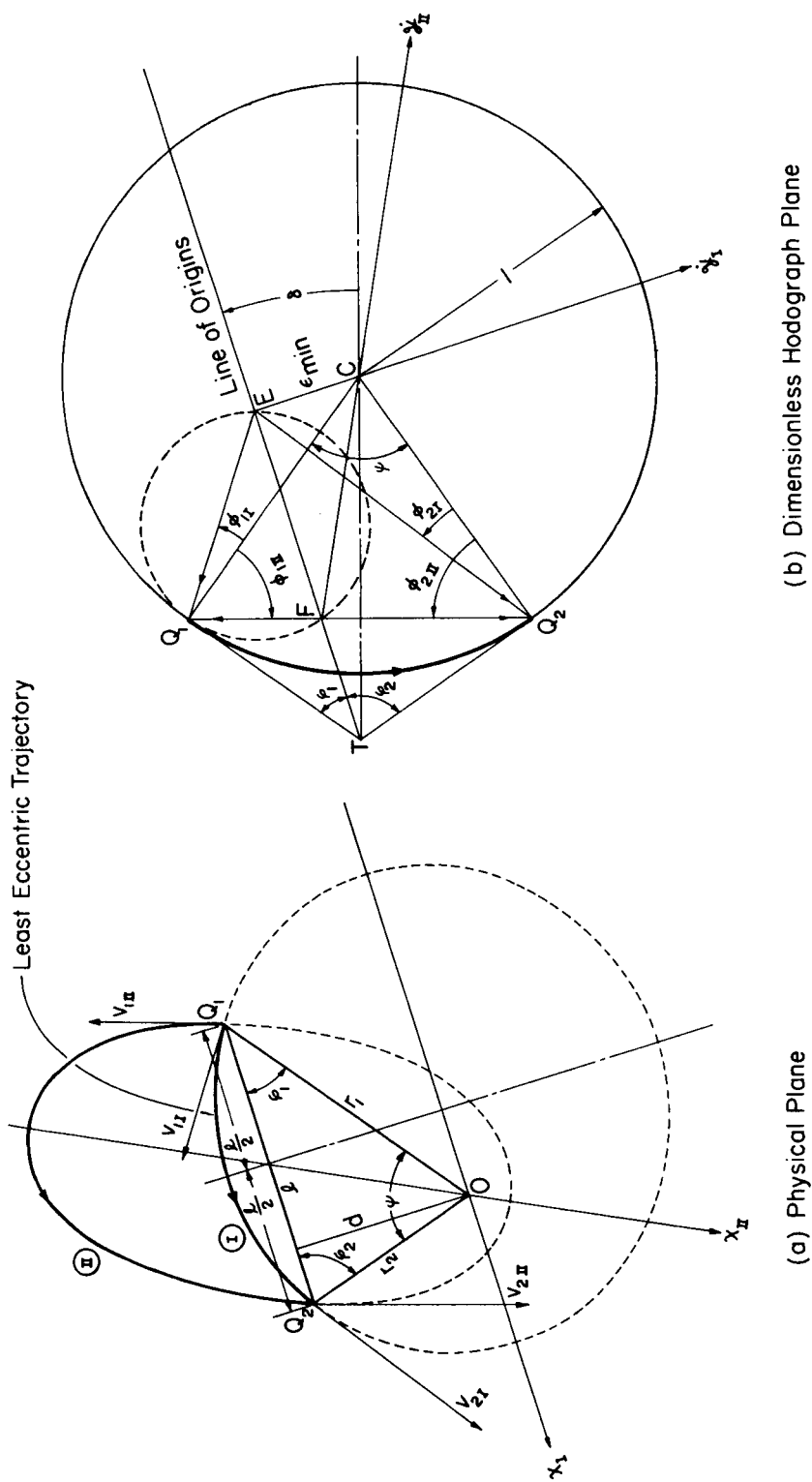


FIGURE 7. THE LEAST ECCENTRIC TRAJECTORY AND ITS CONJUGATE, RANGE $< 180^\circ$.

the orbital points diametrically opposite on an elliptic orbit are connected by*

$$\lambda_1^2 + \lambda_2^2 = 1 \quad (54)$$

which, when combined with the general relation (2), yields

$$\lambda_1^2 = \frac{n}{n+1}, \quad \lambda_2^2 = \frac{1}{n+1} \quad (55)$$

The semimajor axis and the orbital energy of either trajectory are then given by

$$a = \frac{1}{2} (r_1 + r_2) \quad (56)$$

$$k = - \frac{\mu}{r_1 + r_2} \quad (57)$$

Thus the terminal speeds, the major axis, and the orbital energy of a least eccentric trajectory or its conjugate all depend on r_1 and r_2 only, and independent of the vertex angle ψ .

OTHER TRAJECTORIES

In addition to the few particular trajectories analyzed above there are some other ones which might be of interest. For example, associated with the point H_1 , the intersection of the line of origins with the radius OQ_1 (or its extension, see Table 5), the trajectory is one of horizontal departure, since the initial path angle is zero as indicated by the hodograph. Such trajectory will have its apsidal axis coinciding with the initial terminal radius OQ_1 in the physical plane; and the point Q_1 will be its pericenter if $r_1 < r_2$, or apocenter if $r_1 > r_2$. Similarly, associated with the point H_2 , where the line of origins crosses the radius OQ_2 (or its extension) the trajectory will have its final path angle equal to zero. Its apsidal axis will coincide with the final terminal radius OQ_2 and the point Q_2 will be its apocenter if $r_2 > r_1$ or pericenter if $r_2 < r_1$. In the latter case, if Q_2 is considered as the target point on a spherical surface, the trajectory will be cotangential with the surface, and is known in ballistics as the grazing trajectory. In reentry

*See Ref. 6, p. 174.

problems it represents the limiting trajectory for reentry to be effected. The principal elements of either the trajectory of horizontal departure or the grazing trajectory may be easily obtained from the hodograph.

Generally speaking, particular trajectories of interest depend on the particular problem at hand. Complete analysis of all these trajectories is impossible, and their treatment will be left to the separate studies of individual problems.

VII. THE CASE OF 180 DEGREE RANGE

HODOGRAPHIC REPRESENTATION AND GENERAL SURVEY

So far the analysis has been restricted to the case $\psi \neq \pi$. In the boundary case of $\psi = \pi$, the chordal and radial components of the terminal velocities all become parallel, the point T recedes to infinity, and the method of hodograph construction of Section II breaks down. However, the proof for the linear distribution of hodograph origins still stands. With the terminal points Q_1 and Q_2 located on the hodograph circle as usual, obviously the line of origins will be normal to the diameter Q_1Q_2 as shown in Figure 8b. The distance from the center of the hodograph circle to the line of origin is still given by \overline{CE} according to Eq. (5a) which reduces to

$$\overline{CE} = \frac{|1-n|}{1+n} \quad (58)$$

in the present case

In the physical plane the base triangle degenerates into the line segment Q_1Q_2 , which becomes a focal chord; and the normal group and its complement now have the same range angle ψ . In fact, associated with a given chord Q_1Q_2 all distinctions between a normal group and its complement disappear except in the direction of motion. For convenience, however, the same terminology will be retained here by referring to the group moving in the counterclockwise direction as normal, and the other its complement. The hodograph in Figure 8(b) is drawn for the normal group, and the corresponding hodograph for its complement may be obtained by rotating Figure 8(b) through 180° as usual. Following the general survey of Section II and with reference to Figure 8(b), all realistic trajectories will have their origins lying in the open interval from D_{II} via D_I to infinity. Furthermore, the symmetrical nature of the hodograph shows that the conjugate trajectory conics are now identical and symmetrically orientated with respect to the line Q_1Q_2 ; and in fact the conjugate of a trajectory is the reflection of its complement about Q_1Q_2 . The inner forbidden region of departure and outer forbidden region of approach both vanish; the axes of the two limiting hyperbolas both coincide with the normal to the line Q_1Q_2 at O, but point in the opposite directions. The various regions and their included angles are shown in Figure 8a and Table 6. A typical conjugate pair and the corresponding hodograph are shown in Figure 9-1, 2 for the elliptic and hyperbolic cases respectively; for the parabolic case, see Figure 8.

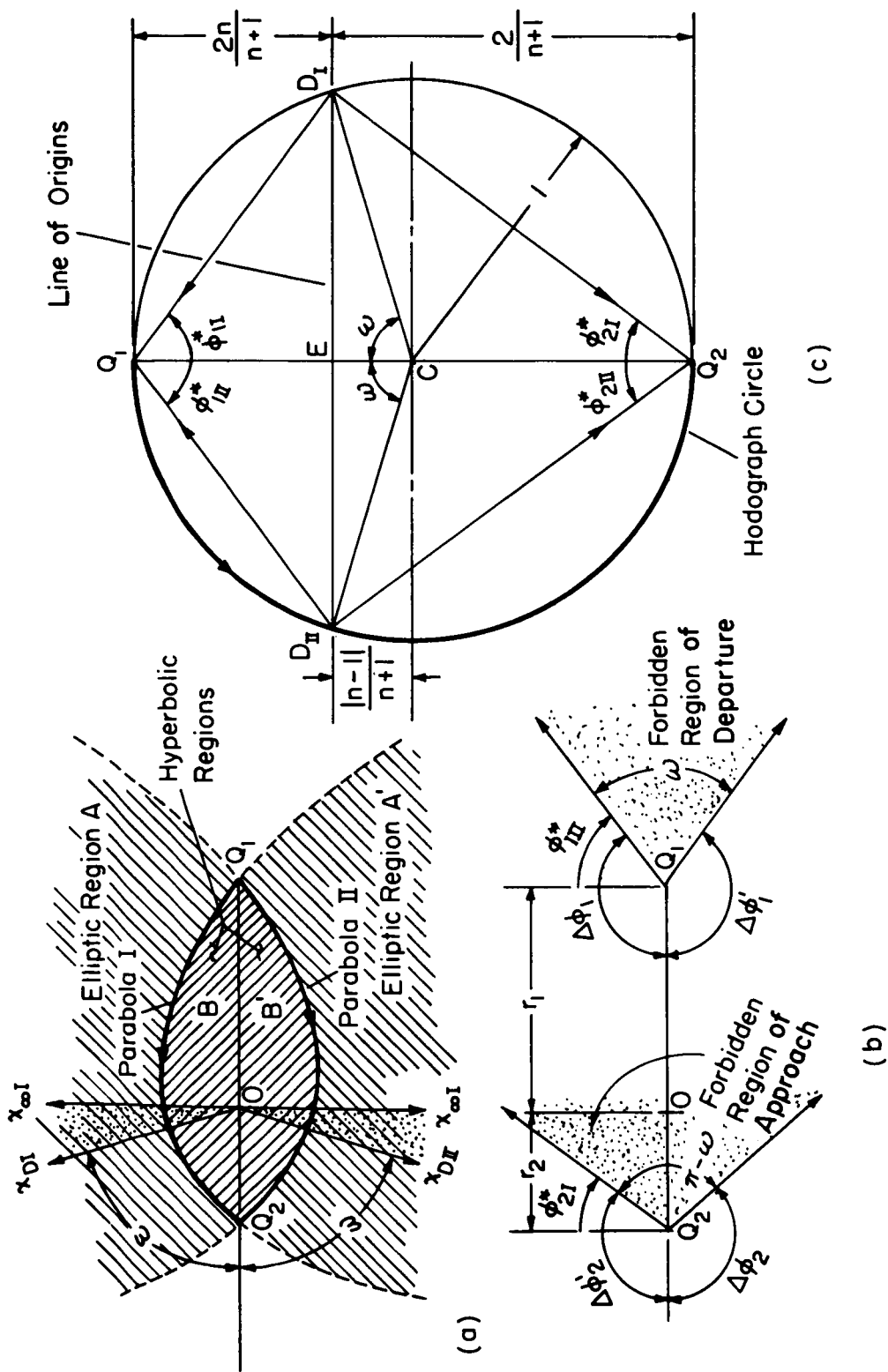


FIGURE 8. SYSTEM OF CO-TERMINAL TRAJECTORIES AND ITS HODO-GRAPHIC REPRESENTATION, 180° RANGE.

Table 6

Possible and Forbidden Regions of Departure and Approach, $\psi = \pi$

Initial Terminal	Final Terminal
<u>Limiting Directions of Departure</u> $(\phi_1)_{UL} = -(\phi_1')_{LL} = \frac{1}{2}(\pi - \omega) (= \phi_1^{*II})$ $(\phi_1)_{LL} = -(\phi_1')_{UL} = -\frac{\pi}{2}$ <u>Possible Regions of Departure</u> $\Delta\phi_1 = \Delta\phi_1' = (\phi_1)_{UL} - (\phi_1)_{LL} = \pi - \frac{\omega}{2}$ Total $\Delta\phi_1 + \Delta\phi_1' = 2\pi - \omega$ <u>Forbidden Region of Departure</u> Included Angle = ω	<u>Limiting Directions of Approach</u> $(\phi_2)_{UL} = -(\phi_2')_{LL} = \frac{\pi}{2}$ $(\phi_2)_{LL} = -(\phi_2')_{UL} = -\frac{\omega}{2} (= \phi_2^{*I})$ <u>Possible Regions of Approach</u> $\Delta\phi_2 = \Delta\phi_2' = (\phi_2)_{UL} - (\phi_2)_{LL} = \frac{1}{2}(\pi + \omega)$ Total $\Delta\phi_2 + \Delta\phi_2' = \pi + \omega$ <u>Forbidden Region of Approach</u> Included Angle = $\pi - \omega$

THE CHARACTERISTICS OF THE CONJUGATE TRAJECTORIES AND THEIR PRINCIPAL ELEMENTS

Although the chordal and radial velocity components are no longer significant in dealing with the 180° range trajectories, the previously derived conjugate relations are preserved. Of course the constant in Eq. (17) or (21) goes to infinity as ψ approaches π ; however, the constant in Eq. (23) or (25) does approach a finite limit. To see this we write the trigonometric identity

$$d \cdot \tan \frac{\psi}{2} = \frac{2r_1 r_2}{l} \sin^2 \frac{\psi}{2} \quad (59)$$

and find

$$\lim_{\psi \rightarrow \pi} d \cdot \tan \frac{\psi}{2} = \frac{2r_1 r_2}{r_1 + r_2} \quad (60)$$

Consequently the conjugate relations (23) and (25) reduce to

$$h_I h_{II} = \frac{2\mu r_1 r_2}{r_1 + r_2} \quad (61)$$

$$\bar{r}_I \bar{r}_{II} = \frac{4r_1^2 r_2^2}{(r_1 + r_2)^2} \quad (62)$$

for the present case. In fact, at this point we may go one step further: since, as pointed out earlier, the conjugate trajectories are now of identical conics, we have

$$h_I = h_{II}, \quad \bar{r}_I = \bar{r}_{II} \quad (63)$$

which, when combined with Eqs. (61) and (62), give immediately the expressions for the angular momentum and the semi-latus rectum as shown in Table 4.

Noting that $\phi_1 = \phi_2 = 0$ when $\psi = \pi$, the conjugate relations (28) now become

$$\begin{aligned} \phi_{1I} + \phi_{1II} &= 0 \quad \text{or} \quad \phi_{1I} = -\phi_{1II} \\ \phi_{2I} + \phi_{2II} &= 0 \quad \text{or} \quad \phi_{2I} = -\phi_{2II} \end{aligned} \quad (64)$$

which are also evident from the symmetry of the present hodograph. To evaluate the terminal path angles we note from the hodograph that, in the right triangles $Q_1O_1B_1$ and Q_1O_1E (Figures 9-1, 2),

$$\overline{Q_1O_{II}} = 2\lambda_1^2 \cos \phi_{1II}, \quad \overline{Q_1O_I} \cos \phi_{1II} = \frac{2n}{n+1}$$

from which by eliminating Q_1O_{II} we obtain

$$\cos \phi_{1II} = \frac{1}{\lambda_1} \sqrt{\frac{n}{n+1}} \quad (65-II)$$

And in view of Eq. (64) we may write

$$(\phi_1) = \pm \cos^{-1} \left(\frac{1}{\lambda} \sqrt{\frac{n}{n+1}} \right) \quad (65)$$

A similar expression stands for the conjugate values of ϕ_2 . Note that the same results here may be obtained by setting $\psi = \pi$ in Eq. (41-a). This shows that the formulas (41-a,b) originally deduced for the case $\psi = \pi$ holds also in the limiting case of $\psi = \pi$. Note here the special case of parabolic flight. The geometry of the hodograph shows that

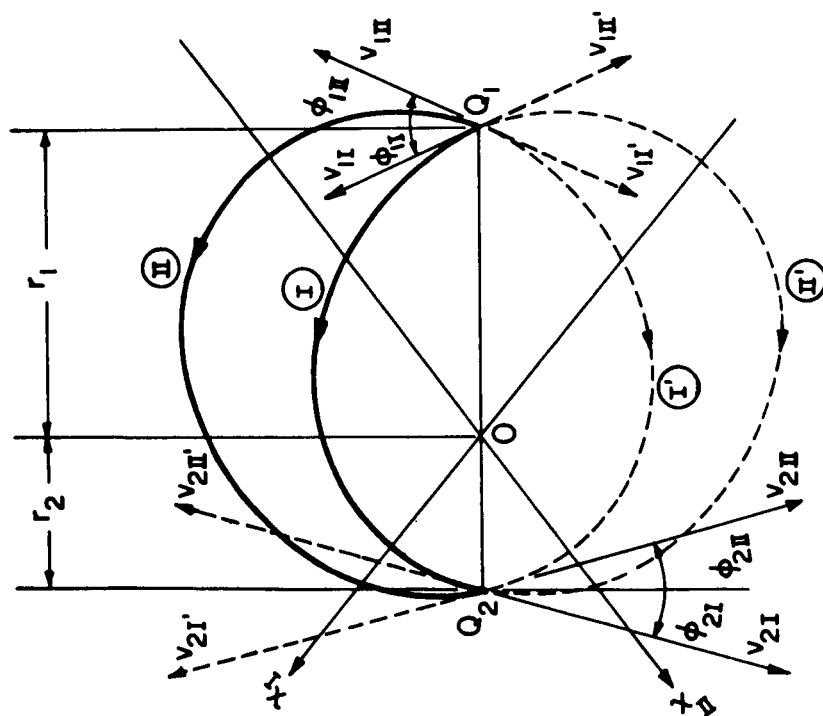
$$|\phi_1^*| + |\phi_2^*| = \frac{\pi}{2} \quad (66)$$

for either group. That is, the terminal velocities in a 180° parabolic flight are normal to each other. Geometrically this implies that the two tangents at the ends of a focal chord of a parabola are orthogonal. This is in fact a geometrical property of a parabola.

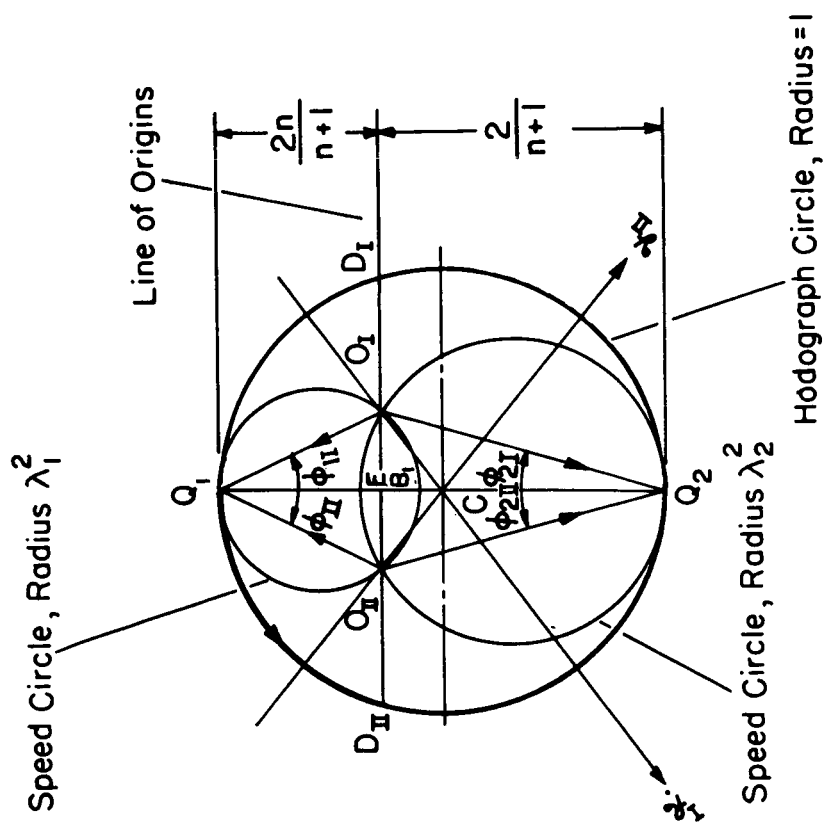
Returning to the general case it is to be noted that, for a 180° flight, between fixed terminals, although the initial speed may be arbitrary, its θ -component is not. This can be seen from the hodograph since

$$\lambda_{\theta 1}^2 = \frac{1}{2} \overline{Q_1E} = \frac{n}{n+1} \quad (67)$$

which shows that $\lambda_{\theta 1}$ and consequently $V_{\theta 1}$ is fixed by the terminal distances



(a) Physical Plane



(b) Dimensionless Hodograph Plane

FIGURE 9-1. THE CONJUGATE ELLIPTIC TRAJECTORIES, 180° RANGE.

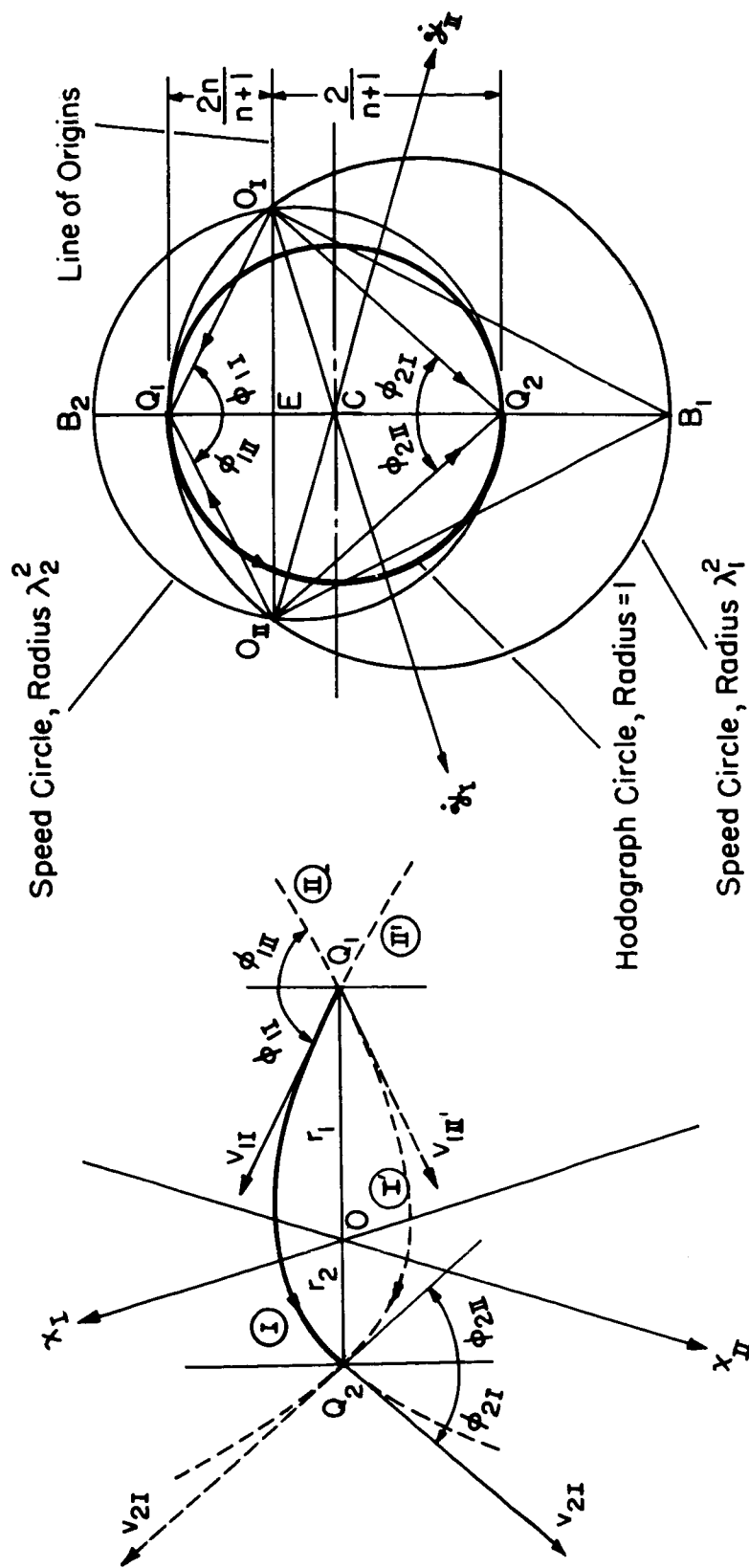


FIGURE 9-2. THE CONJUGATE HYPERBOLIC TRAJECTORIES, 180° RANGE.

alone, hence independent of the initial speed. The same is true for the final speed $V_{\theta 2}$.

Formulas for other trajectory elements may be likewise deduced from the hodograph geometry of Figures 8 and 9 or by using appropriate orbital relations. The results are summarized in column 3, Table 4; and the dependence of some of the principal trajectory elements on the distance ratio and the initial speed are shown graphically in Figures 11-1, 2(d). It is worth noting from Table 4 that, for $\psi = \pi$, in addition to the θ -components of the terminal velocities, the angular momentum and latus rectum are also fixed by the terminal distances r_1 and r_2 alone, hence they are independent of the initial speed, or the particular choice of trajectory.

The criteria given in Table 5 for the occurrence of apses on the trajectory still stand for the present case. However, it is to be noted that, as the present hodograph shows, the points H_1 and H_2 coincide at E. This indicates that at least one of the two apses will lie on the trajectory, and both will be on the trajectory when the origin is at E, corresponding to the minimum energy trajectory.

Finally, for a 180° -flight, the parameters η_0 and η'_0 in Lambert's formula all vanish and the resulting simplified expressions for the duration of flight are given in Appendix B and graphically shown in Figure 11-3(d). It only needs to mention here that, in the elliptic case,

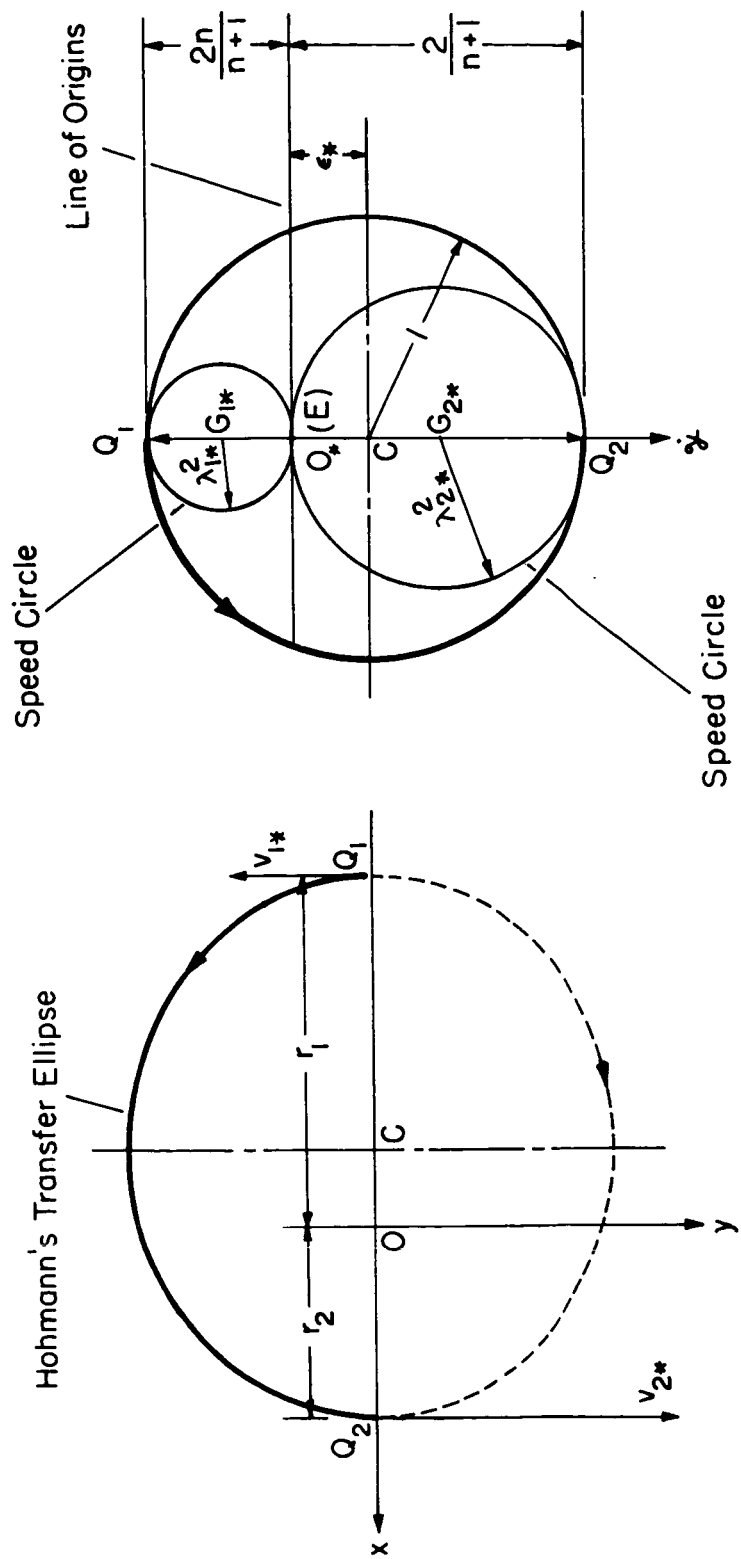
$$\Delta t_I + \Delta t_{II} = \frac{2\pi}{\sqrt{\mu}} \left(\frac{r_1}{2(1-\lambda_1^2)} \right)^{3/2} = \tau \quad (\text{period of elliptic motion}) \quad (68)$$

as it should be since as pointed out earlier, the conjugate path is only the reflection of the complementary path about the line Q_1Q_2 .

THE MINIMUM ENERGY TRAJECTORY AND THE LEAST ECCENTRIC TRAJECTORY

When $\psi = \pi$ the minimum energy trajectory and the least eccentric trajectory coincide, both have the point E as their hodograph origin (see Figure 10). The trajectory is a half ellipse with its apsidal axis coinciding with Q_1Q_2 , and the trajectory conic is the well-known Hohmann's ellipse. Thus a Hohmann's ellipse is not only the least energetic, but also the least eccentric, among all trajectories of common terminals with 180° range. From Eqs. (57) and (58) the orbital energy and the eccentricity of a Hohmann's ellipse are found to be

$$k_* \Big|_{\psi = \pi} = - \frac{\mu}{r_1 + r_2} \quad (69)$$



(a) Physical Plane

(b) Dimensionless Hodograph Plane

FIGURE 10. THE MINIMUM ENERGY AND LEAST ECCENTRIC TRAJECTORY, 180° RANGE.

and

$$\epsilon_* \Big|_{\psi = \pi} = \frac{|1-n|}{1+n} \quad (70)$$

Comparing these formulas with the corresponding general formulas (49) and (5-a) respectively, we see that, if the terminal distances are fixed, but the range angle is allowed to vary, the energy of the Hohmann's ellipse is in fact the greatest among all the minimum energy ones; while its eccentricity is the overall minimum in the entire trajectory system. Other elements of the Hohmann's ellipse can be easily obtained from the hodograph as usual.

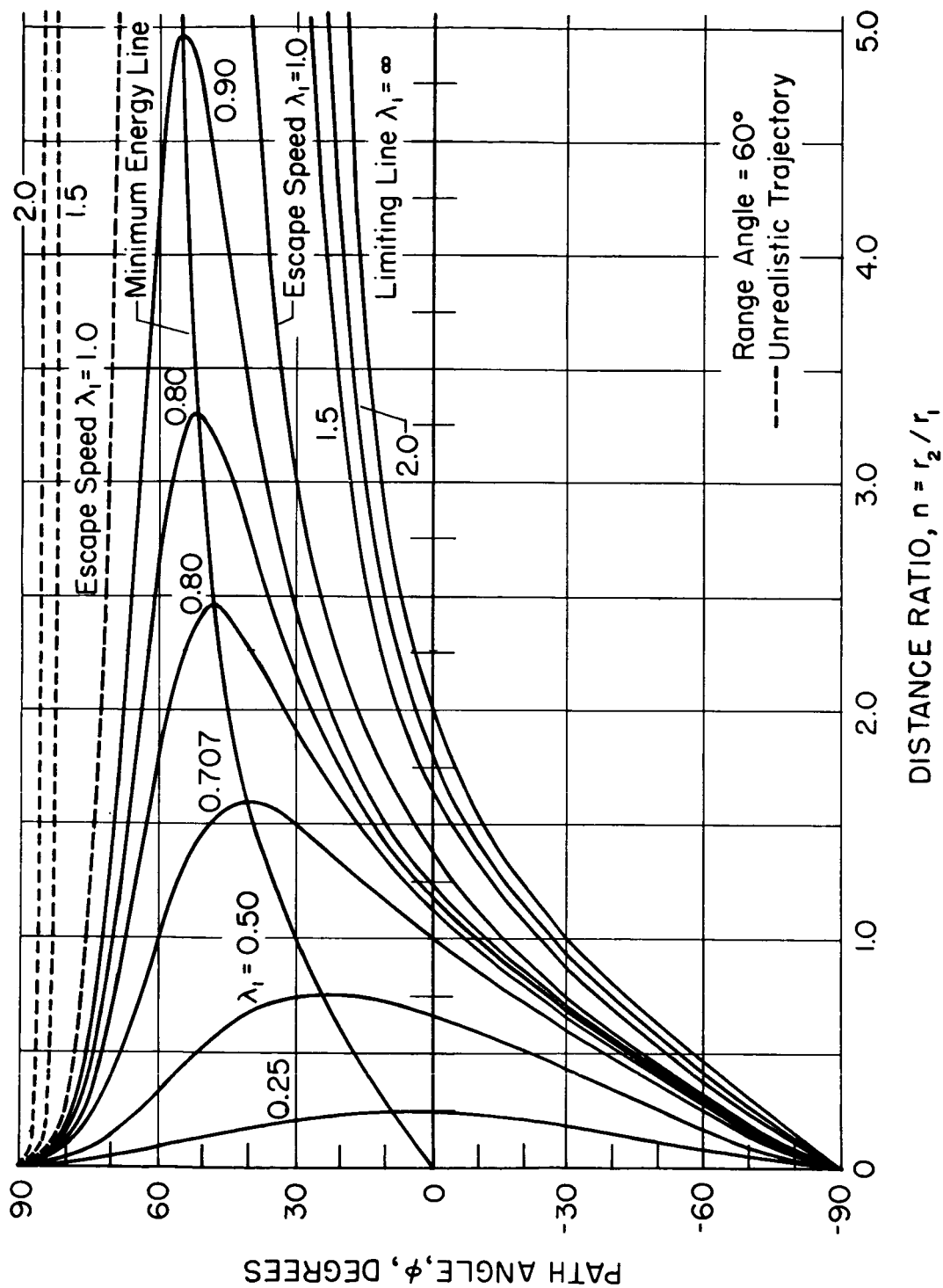


FIGURE 11-1(a). VARIATION OF THE RANGE-CONSTRAINED PATH ANGLE WITH DISTANCE RATIO AND INITIAL SPEED.

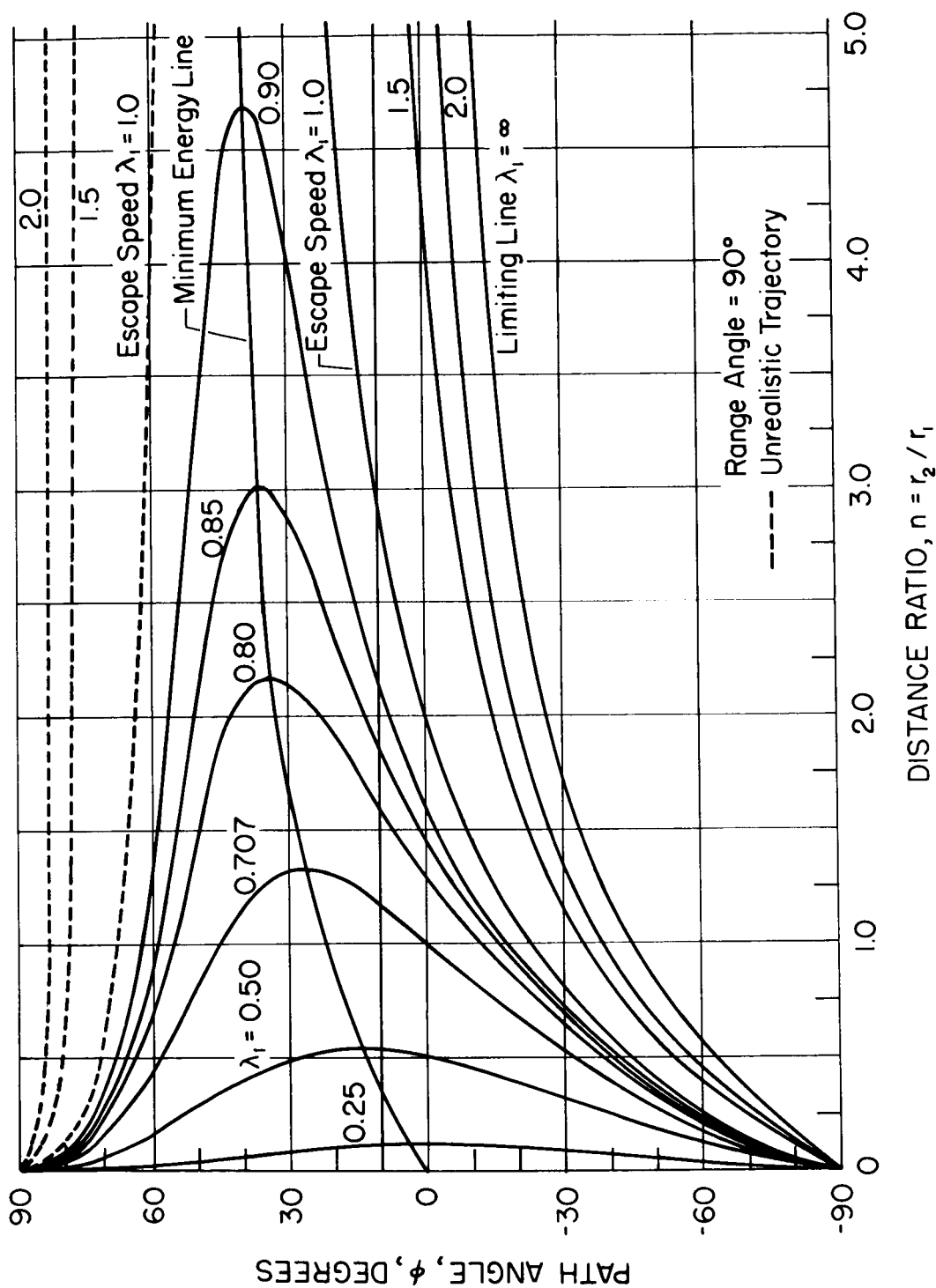


FIGURE 11-1(b). VARIATION OF THE RANGE-CONSTRAINED PATH ANGLE WITH DISTANCE RATIO AND INITIAL SPEED.

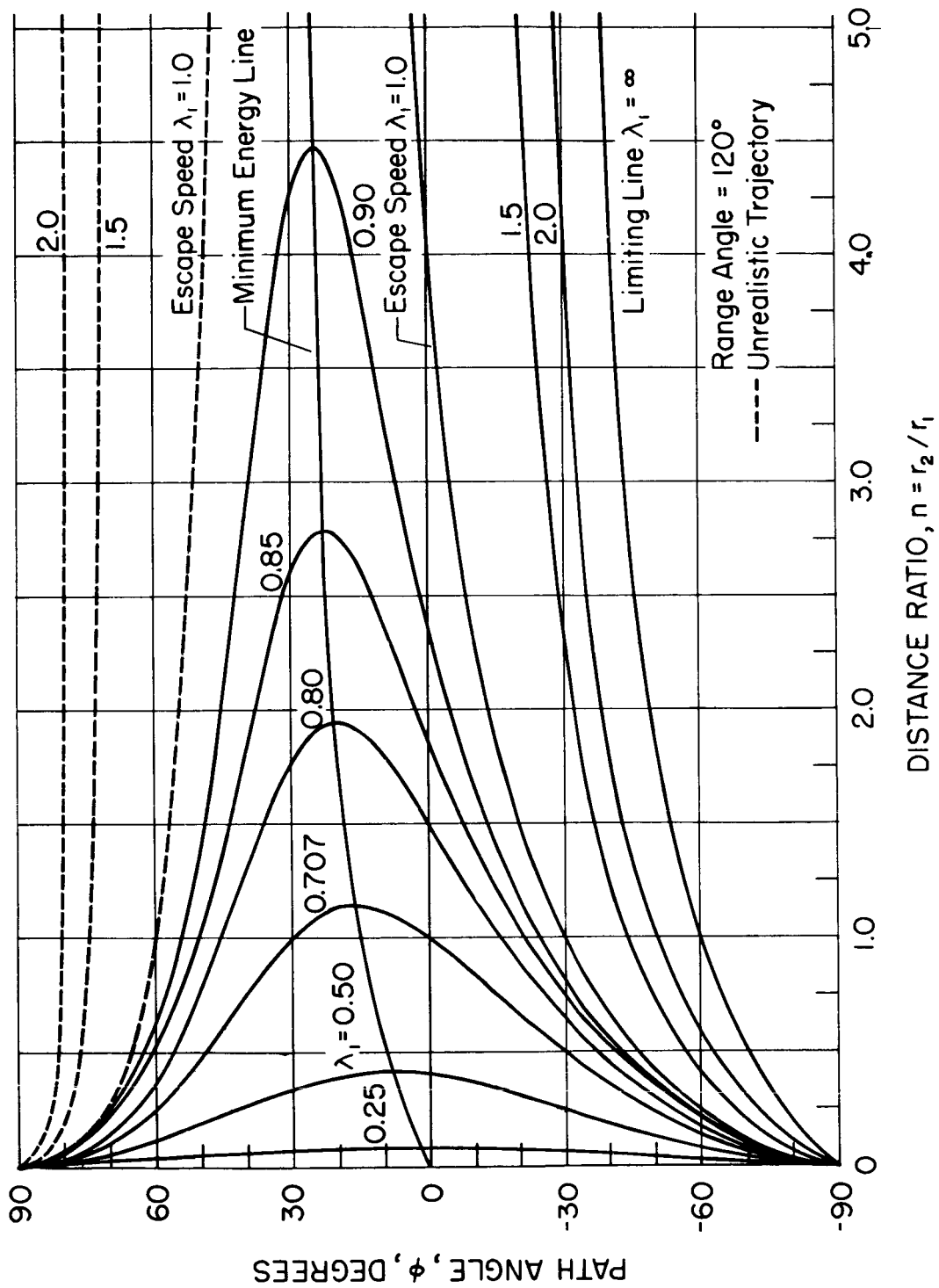


FIGURE 11-1(c). VARIATION OF THE RANGE-CONSTRAINED PATH ANGLE WITH DISTANCE RATIO AND INITIAL SPEED.

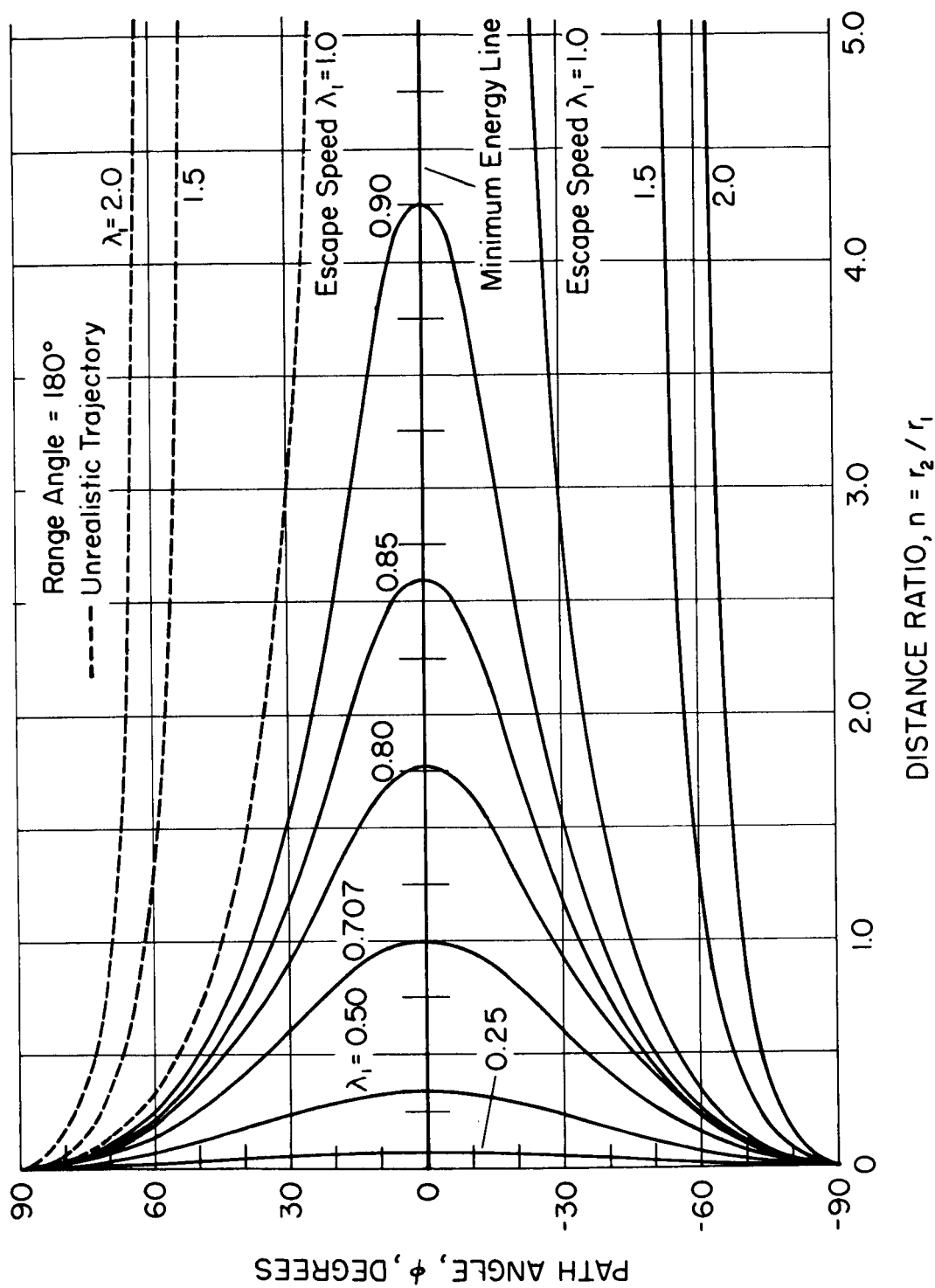


FIGURE 11-1(d). VARIATION OF THE RANGE-CONSTRAINED PATH ANGLE WITH DISTANCE RATIO AND INITIAL SPEED.

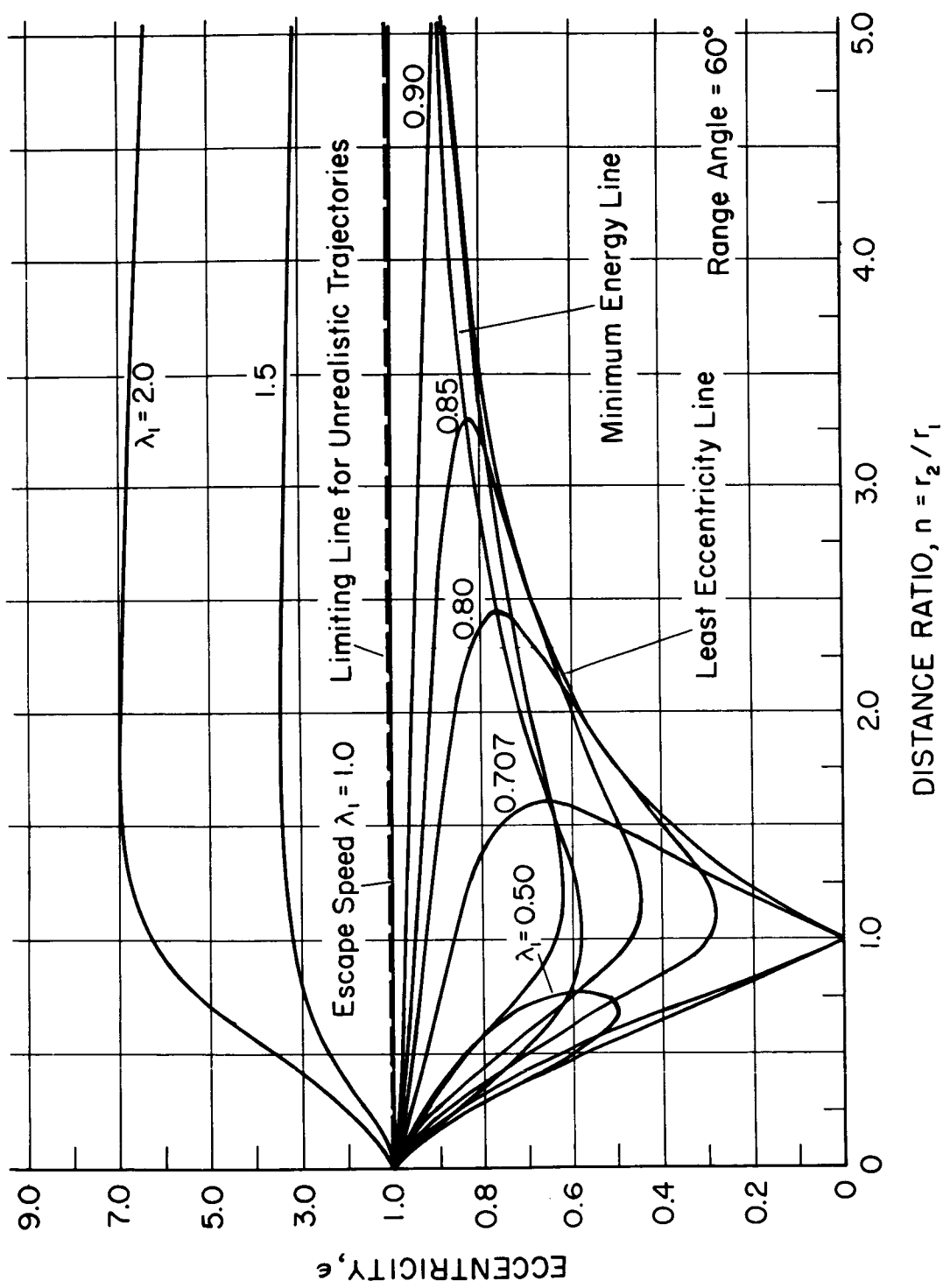


FIGURE II-2(a) VARIATION OF THE RANGE-CONSTRAINED TRAJECTORY ECCENTRICITY WITH DISTANCE RATIO AND INITIAL SPEED.

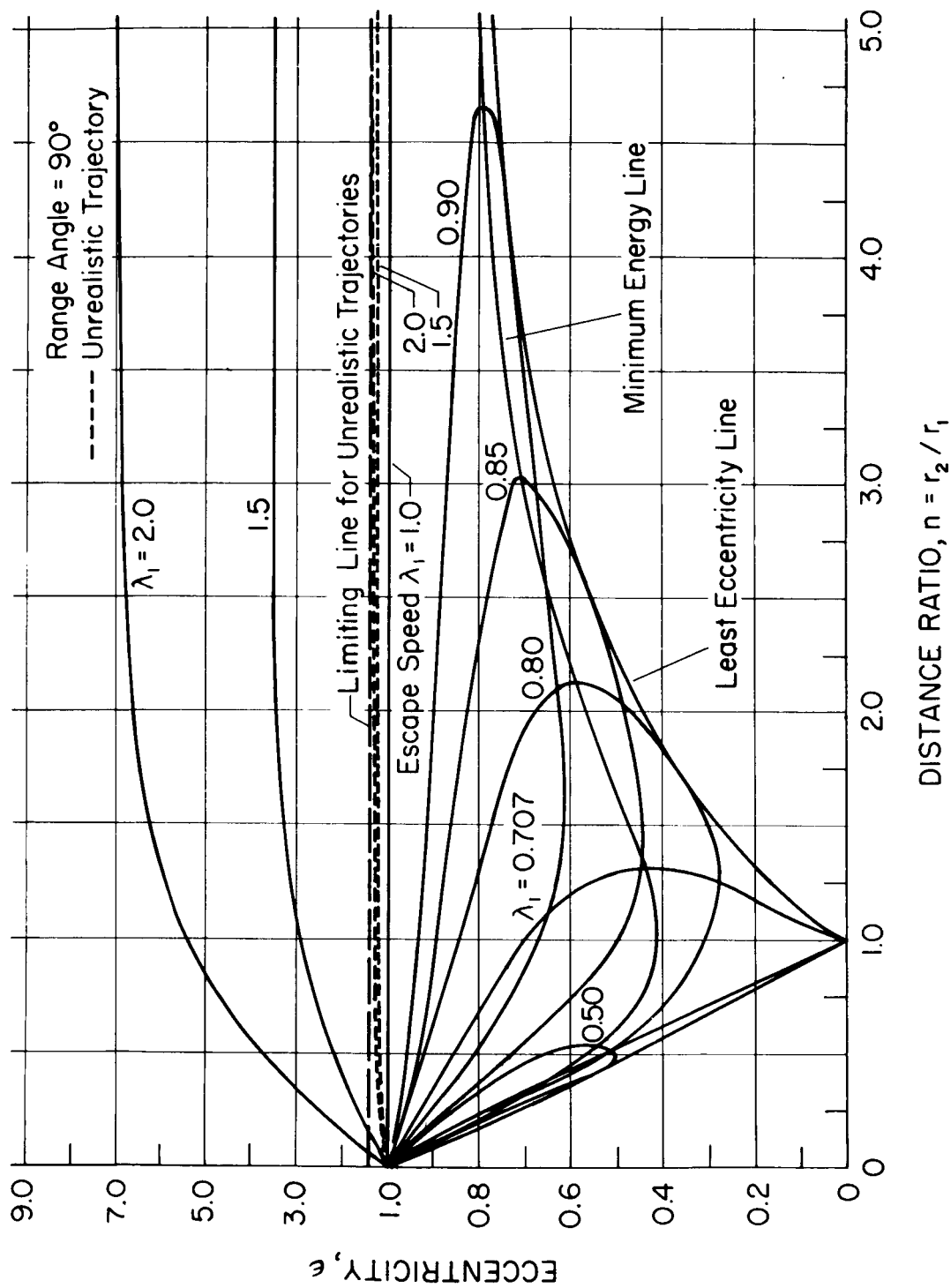


FIGURE 11-2(b). VARIATION OF THE RANGE - CONSTRAINED TRAJECTORY ECCENTRICITY WITH DISTANCE RATIO AND INITIAL SPEED.

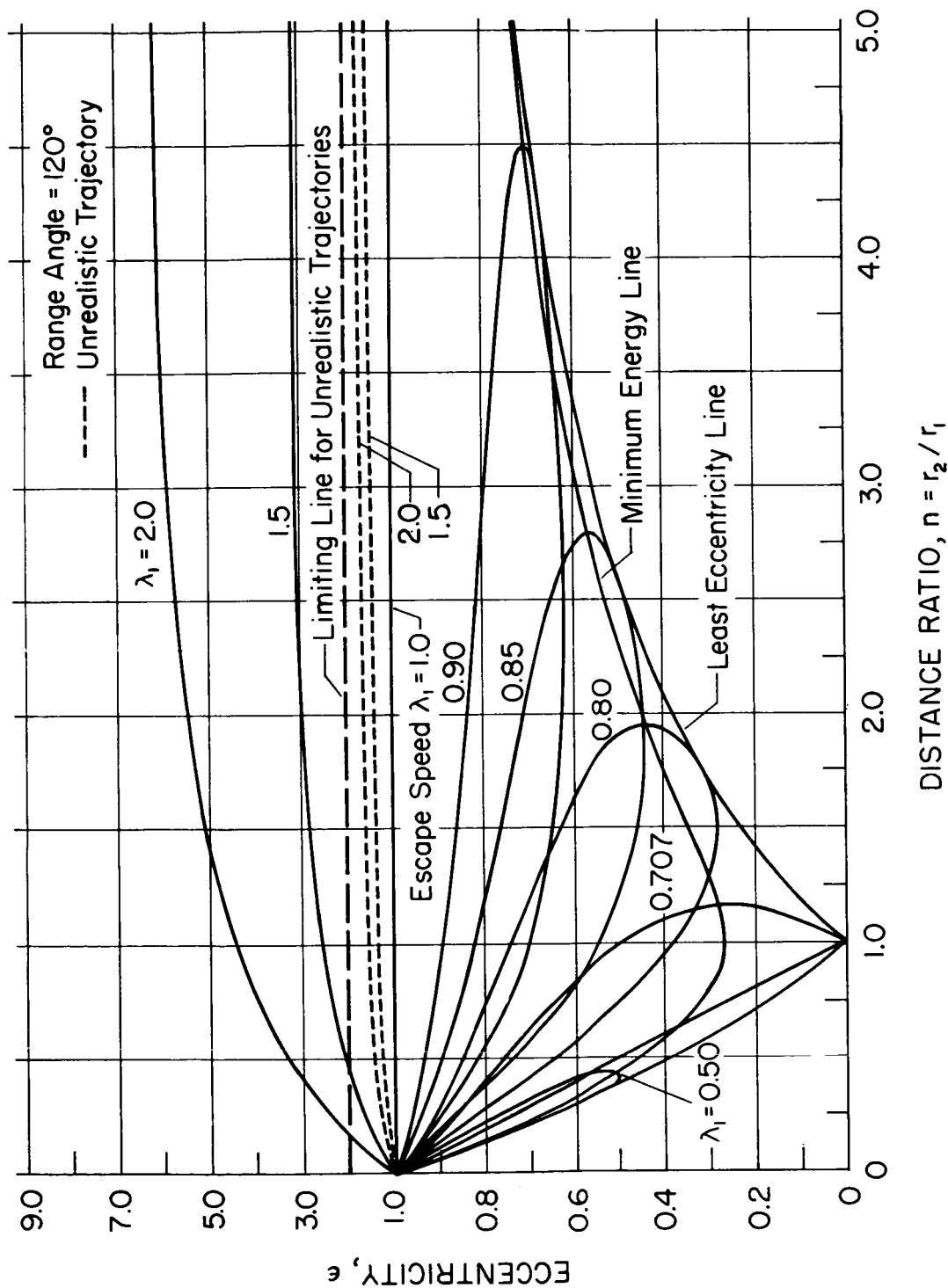


FIGURE 11-2(c). VARIATION OF THE RANGE-CONSTRAINED TRAJECTORY ECCENTRICITY WITH DISTANCE RATIO AND INITIAL SPEED.

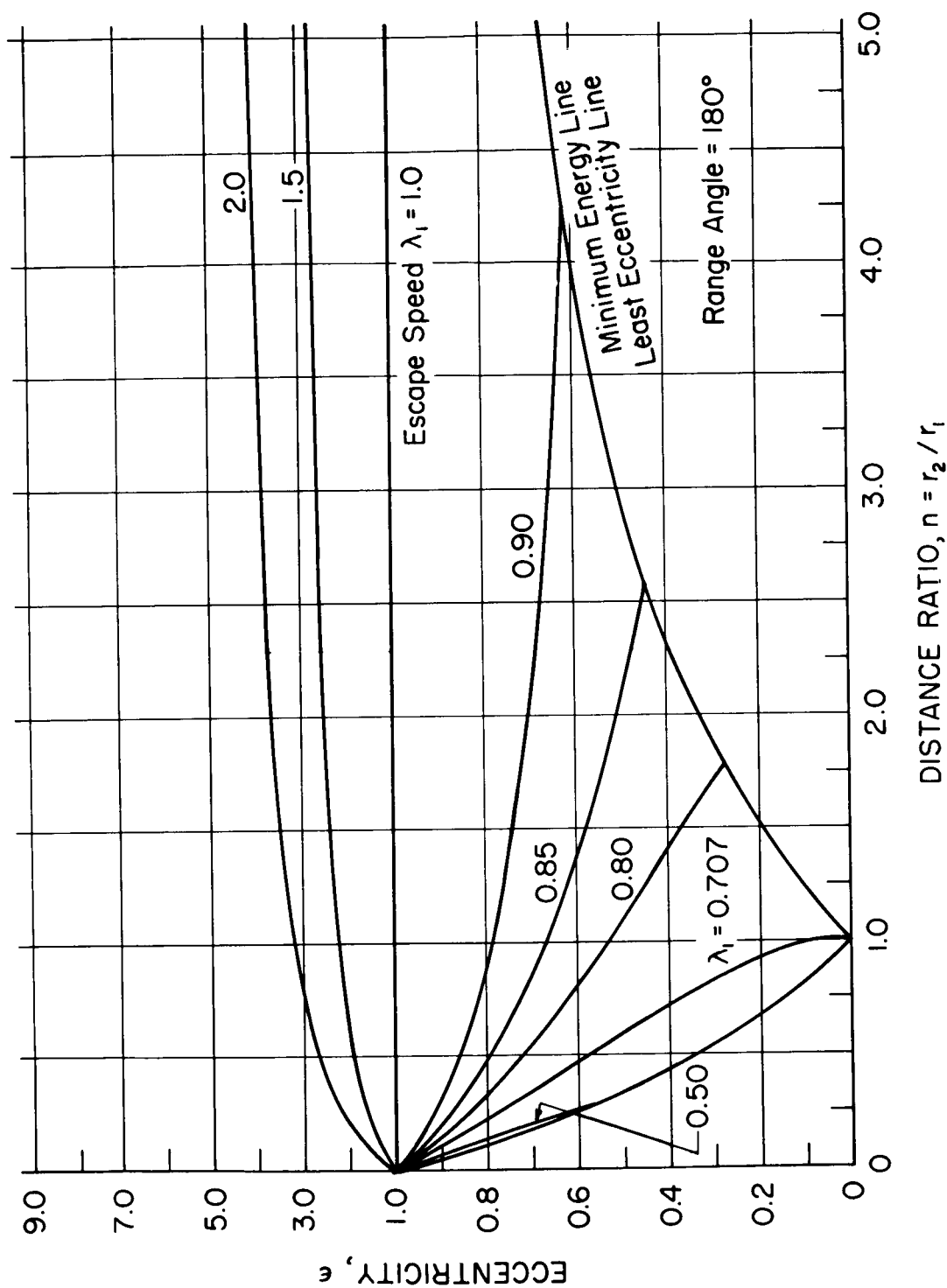


FIGURE 11 - 2(d). VARIATION OF THE RANGE - CONSTRAINED TRAJECTORY ECCENTRICITY WITH DISTANCE RATIO AND INITIAL SPEED.

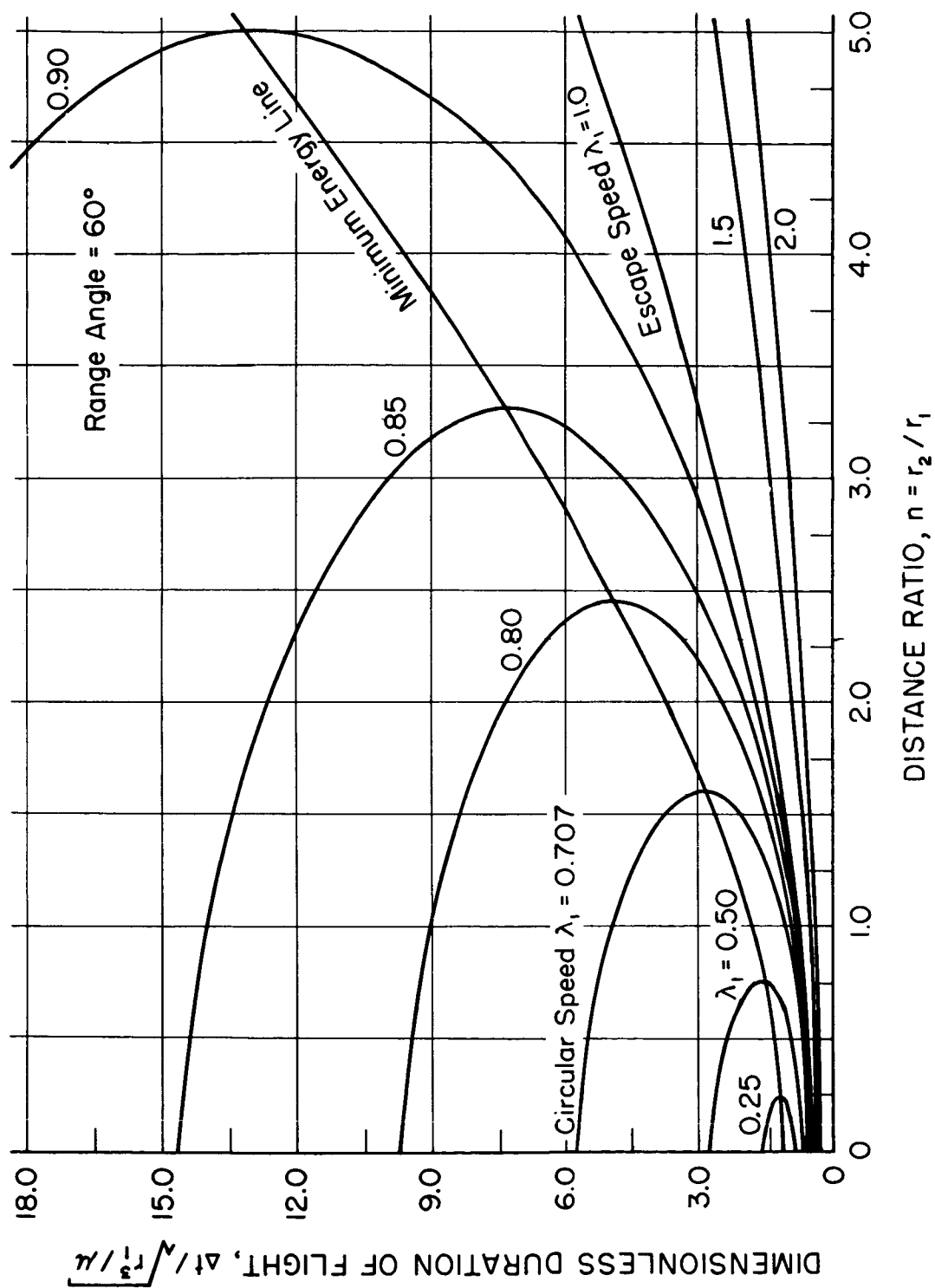


FIGURE 11-3(a) VARIATION OF THE DURATION OF TERMINAL-TO-TERMINAL FLIGHT WITH DISTANCE RATIO AND INITIAL SPEED.

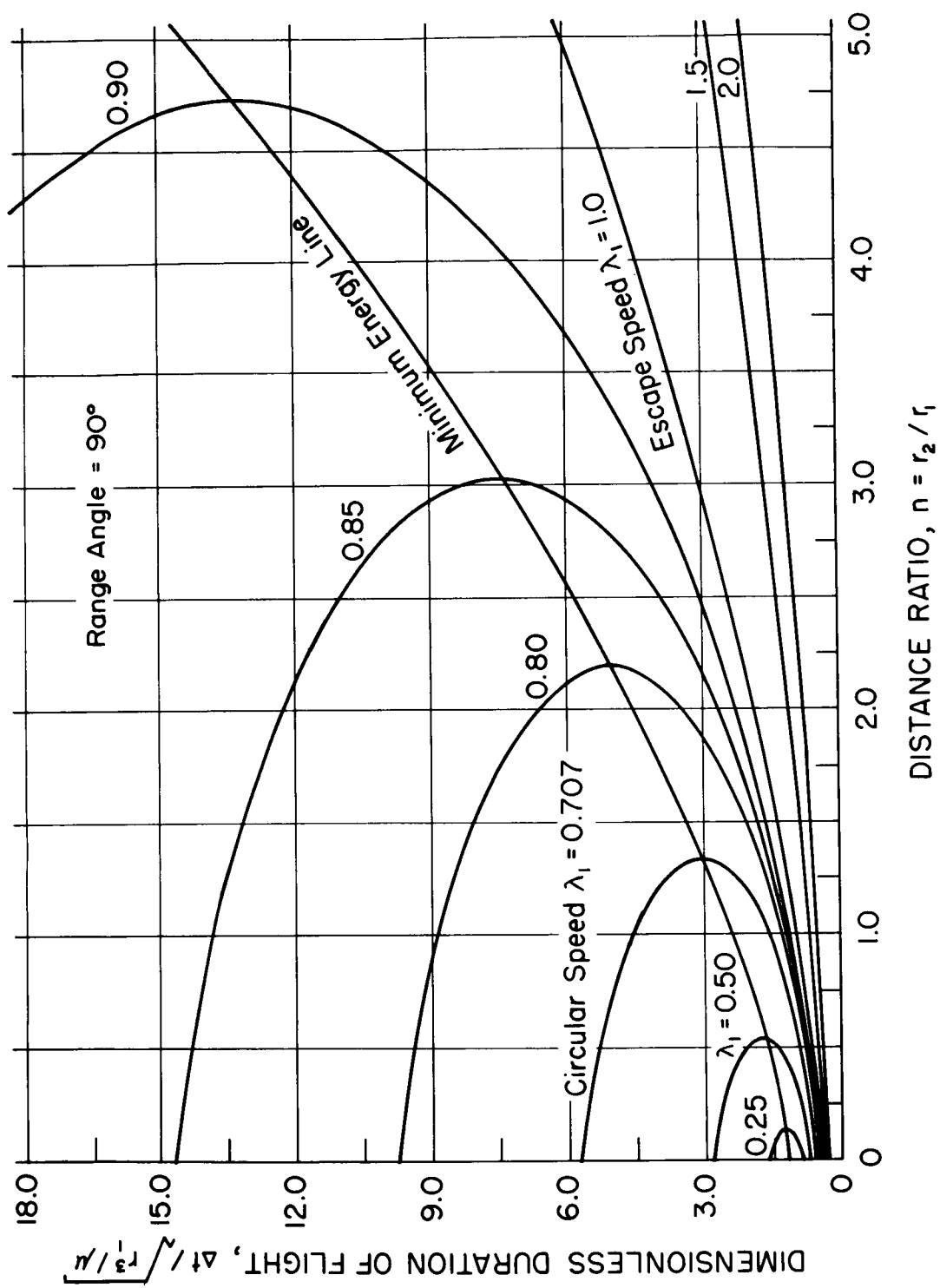


FIGURE 11 - 3(b) VARIATION OF THE DURATION OF TERMINAL-TO-TERMINAL FLIGHT WITH DISTANCE RATIO AND INITIAL SPEED.

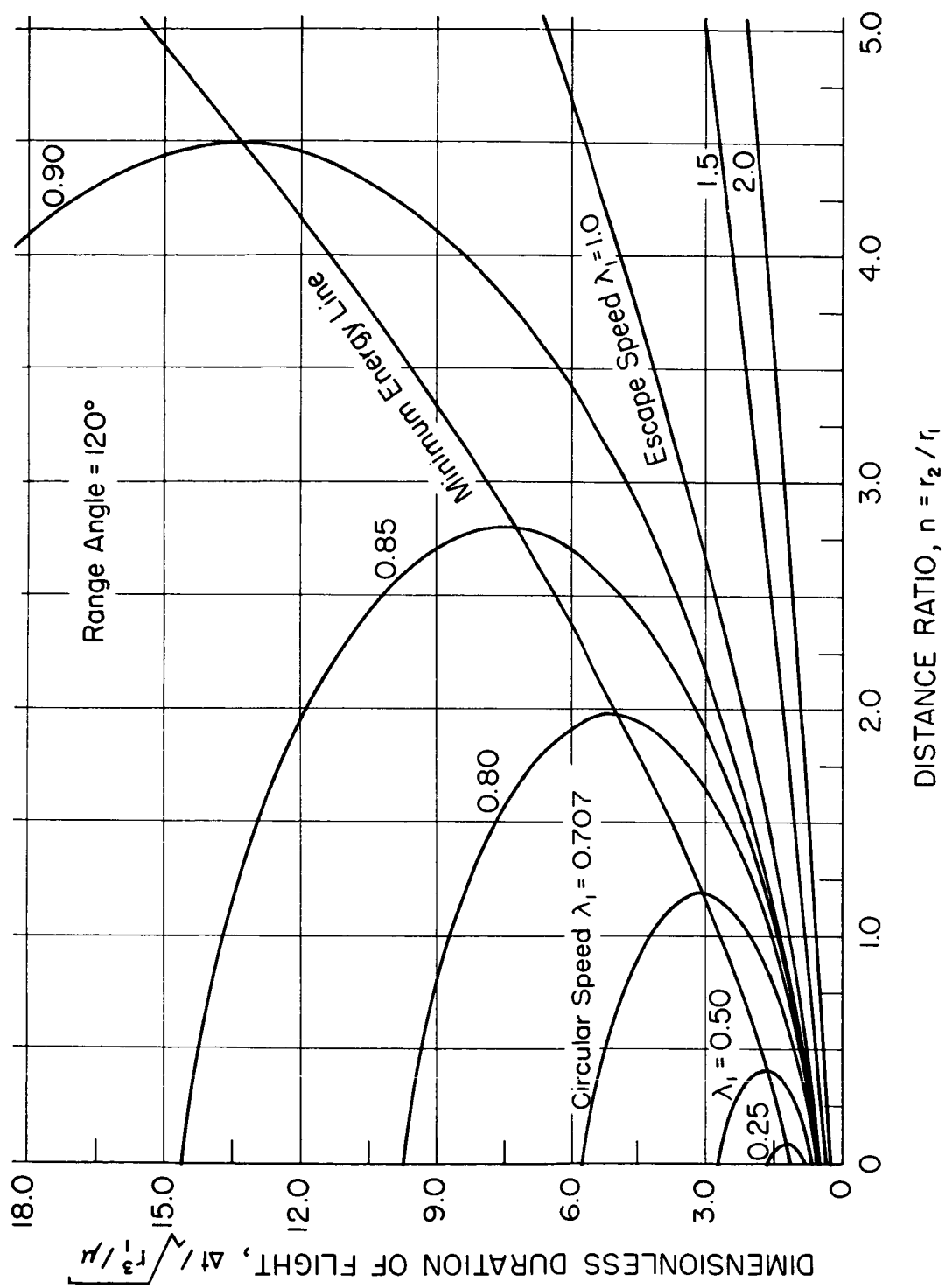


FIGURE 11 - 3(c) VARIATION OF THE DURATION OF TERMINAL - TO - TERMINAL FLIGHT WITH DISTANCE RATIO AND INITIAL SPEED.

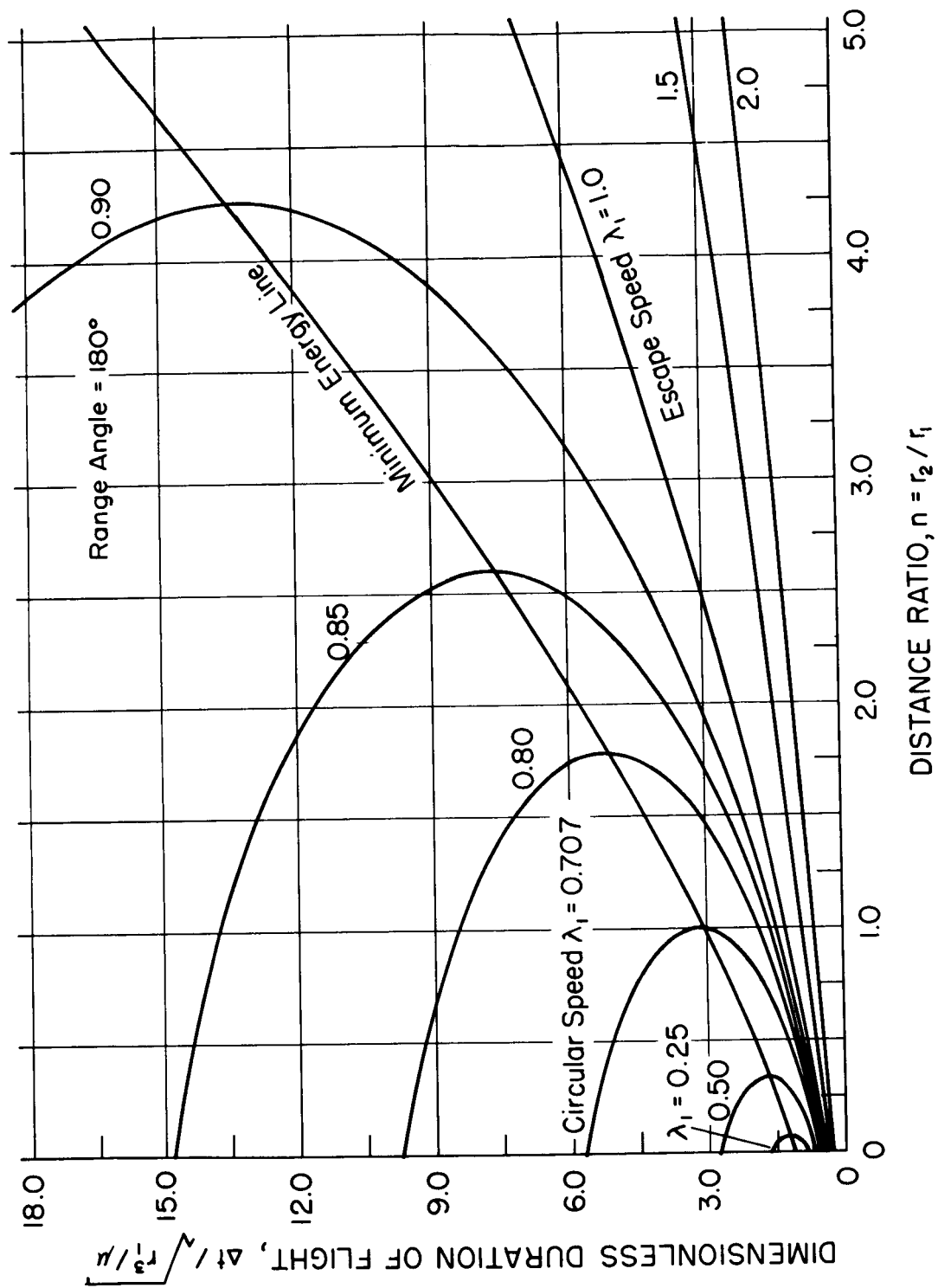


FIGURE 11-3(d) VARIATION OF THE DURATION OF TERMINAL-TO-TERMINAL FLIGHT WITH DISTANCE RATIO AND INITIAL SPEED.

VIII. SUMMARY OF CONCLUSIONS

The main conclusions obtained in the present analysis may be summarized as follows:

1. For a system of all co-terminal trajectories of the same range angle, the locus of the hodograph origin in the dimensionless x, y -plane is a straight line parallel to the line connecting the terminal points in the physical plane. This is true regardless of whether the range angle is less than, greater than or equal to π .

2. Of the infinitely many co-terminal trajectories associated with a given base triangle in a given field:

(a) Only two are parabolic, and all the realistic trajectories, elliptic and hyperbolic, are confined in the region outside the base triangle and bounded between the branches of the parabolas extending from each terminal to infinity, with those of the normal group all above the chord or base (Q_1Q_2) of the base triangle and the complementary group in the rest of the region (see Figure 3(a)).

(b) There exist an upper limit and a lower limit for the initial path angle in each group beyond which no such trajectory is possible; consequently, there is a forbidden angular region for the directions of departure at the initial terminal. A similar situation exists for the directions of approach at the final terminal. The included angle of each region is determined by the geometry of the base triangle (see Figure 3 and Table 2).

(c) The positive portions of the elliptic apsidal axes, and those of the hyperbolic apsidal axes are also confined in certain angular regions bounded by the apsidal axes of the two parabolic trajectories and the two axes coinciding with the base altitude and the bisector of the vertex angle ψ of the base triangle respectively. The included angle of each region is also determined by the geometry of the base triangle (see Figure 3 and Table 3).

(d) Besides the well-known minimum speed, there exists a least elliptic eccentricity which the trajectory may attain, and an upper limit for the hyperbolic eccentricity of the complementary group (see Eqs. (5,5a) and (7)). There is no upper limit for the hyperbolic eccentricity of the normal group.

3. For a pair of conjugate trajectories associated with a given base triangle and an arbitrary initial speed in a given field:

(a) The chordal and radial components of the terminal velocity of one trajectory are equal to the radial and chordal components of the terminal

velocity of the other respectively (the reciprocal relation).

(b) The product of each conjugate pair of the following quantities is a constant:

- i. The chordal component of the terminal velocity.
- ii. The radial component of the terminal velocity.
- iii. The angular momentum.
- iv. The latus rectum.

Each constant depends of the vertex angle ψ and the base altitude d alone, hence independent of the initial speed.

(c) The sum of the conjugate path angles at either terminal is a constant, equal to one-half of the base angle at that terminal.

4. A minimum energy trajectory is characterized by the following features:

(a) The chordal and radial components of either terminal velocity are equal.

(b) The direction of motion at either terminal bisects any pair of conjugate directions at that terminal. This direction depends only on the base angle at that terminal (see Eqs. (46)).

(c) The chordal and radial components of the terminal velocity, the angular momentum, and the latus rectum are the geometrical mean of the conjugate pair of the corresponding quantities associated with a base triangle of the same vertex angle ψ and base altitude d .

5. A least eccentric trajectory is characterized by the following features:

(a) The apsidal axis of the trajectory ellipse is parallel to the chord Q_1Q_2 .

(b) The terminal speed parameters, the major axis, and the orbital energy all depend on the terminal distances only, hence independent of the range angle.

(c) The least eccentricity is proportional to the numerical difference between the terminal distances and inversely proportional to the length of the chord (see Eq. (5-a)).

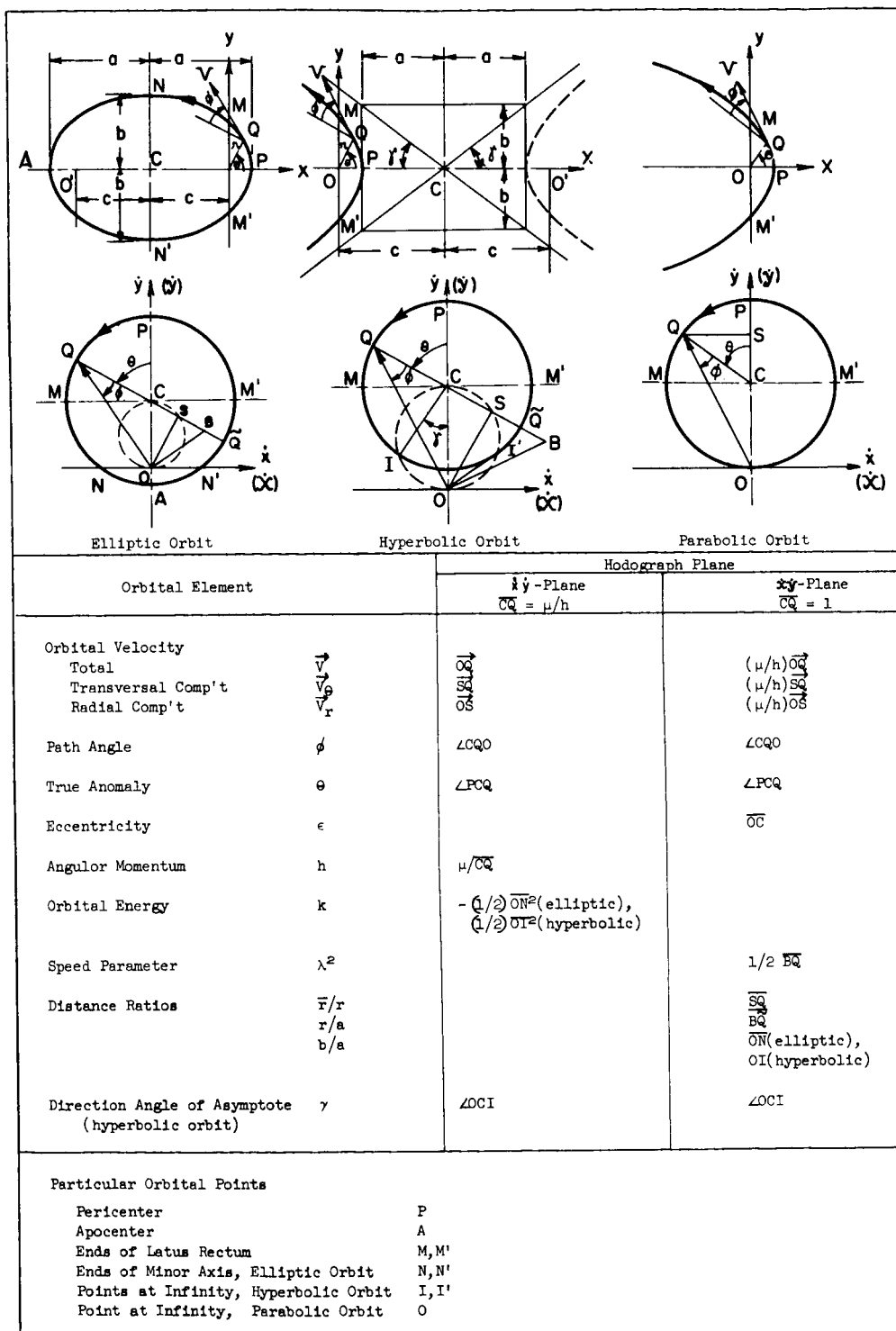
6. In the case of 180° range, the θ -components of the terminal velocities, the angular momentum and the latus rectum are all fixed by the terminal distances r_1 and r_2 alone, thus they are independent of the initial speed, hence the choice of trajectory.

7. (a) In a system of co-terminal trajectories of 180° range the Hohmann's ellipse has both the minimum orbital energy and the least eccentricity.

(b) In a system of fixed terminal distances but varying range angle, the Hohmann's ellipse has the greatest minimum energy and the overall least eccentricity.

APPENDIX A

CORRELATION BETWEEN THE PHYSICAL PLANE AND THE HODOGRAPH PLANE FOR THE KEPLERIAN ORBITS*



Note: 1. Positive directions of θ and ϕ are indicated in the figure.

2. $\angle BOQ = 90^\circ$

*Condensed from Ref. 8, pp. 882-894.

APPENDIX B

SUMMARY OF FORMULAS: DURATION OF TERMINAL-TO-TERMINAL FLIGHT

	Range Angle < π	Range Angle > π	Range Angle = π
Elliptic	I $\frac{1}{\sqrt{\mu}} \left[\frac{\Delta_1}{2(1-\lambda_1^2)} \right]^{\frac{3}{2}} [\xi_0 - \eta_0 - \sin \xi_0 + \sin \eta_0]$	$\frac{1}{\sqrt{\mu}} \left[\frac{\Delta_1}{2(1-\lambda_1^2)} \right]^{\frac{3}{2}} [\xi_0 + \eta_0 - \sin \xi_0 - \sin \eta_0]$	$\frac{1}{\sqrt{\mu}} \left[\frac{\Delta_1}{2(1-\lambda_1^2)} \right]^{\frac{3}{2}} [\xi_0 - \sin \xi_0]$
	II $\frac{1}{\sqrt{\mu}} \left[\frac{\Delta_1}{2(1-\lambda_1^2)} \right]^{\frac{3}{2}} [2\pi - \xi_0 - \eta_0 + \sin \xi_0 + \sin \eta_0]$	$\frac{1}{\sqrt{\mu}} \left[\frac{\Delta_1}{2(1-\lambda_1^2)} \right]^{\frac{3}{2}} [2\pi - \xi_0 + \eta_0 + \sin \xi_0 - \sin \eta_0]$	$\frac{1}{\sqrt{\mu}} \left[\frac{\Delta_1}{2(1-\lambda_1^2)} \right]^{\frac{3}{2}} [2\pi - \xi_0 + \sin \xi_0]$
	$\xi_0 = 2 \sin^{-1} \sqrt{\frac{\xi_0^2}{\lambda_1^2} (1-\lambda_1^2)}$	$\eta_0 = 2 \sin^{-1} \sqrt{\frac{\eta_0^2}{\lambda_1^2} (1-\lambda_1^2)}$	$\xi_0 = 2 \sin^{-1} \sqrt{(n+D)(1-\lambda_1^2)}$
Hyperbolic	I $\frac{1}{\sqrt{\mu}} \left[\frac{\Delta_1}{2(\lambda_1^2-1)} \right]^{\frac{3}{2}} [\sinh \xi_0' - \sinh \eta_0' - \xi_0' + \eta_0']$	$\frac{1}{\sqrt{\mu}} \left[\frac{\Delta_1}{2(\lambda_1^2-1)} \right]^{\frac{3}{2}} [\sinh \xi_0' + \sinh \eta_0' - \xi_0' - \eta_0']$	$\frac{1}{\sqrt{\mu}} \left[\frac{\Delta_1}{2(\lambda_1^2-1)} \right]^{\frac{3}{2}} [\sinh \xi_0' - \xi_0']$
	$\xi_0' = 2 \sinh^{-1} \sqrt{\frac{\xi_0'^2}{\lambda_1^2} (\lambda_1^2-1)}$	$\eta_0' = 2 \sinh^{-1} \sqrt{\frac{\eta_0'^2}{\lambda_1^2} (\lambda_1^2-1)}$	$\xi_0' = 2 \sinh^{-1} \sqrt{(n+D)(\lambda_1^2-1)}$
Parabolic	I $\frac{1}{3} \sqrt{\frac{2}{\mu}} [s^{\frac{3}{2}} - (s-l)^{\frac{3}{2}}]$	$\frac{1}{3} \sqrt{\frac{2}{\mu}} [s^{\frac{3}{2}} + (s-l)^{\frac{3}{2}}]$	$\frac{1}{3} \sqrt{\frac{2}{\mu}} \left[\frac{\Delta_1}{2} (n+1) \right]^{\frac{3}{2}}$
Minimum Energy Trajectory (Elliptic)	$\frac{1}{\sqrt{\mu}} \left[\frac{\xi_0^2}{2} \right]^{\frac{3}{2}} \left[\pi - 2 \sin^{-1} \sqrt{\frac{\xi_0^2}{2}} + \frac{2}{3} \sqrt{2(s-l)} \right]$	$\frac{1}{\sqrt{\mu}} \left[\frac{\xi_0^2}{2} \right]^{\frac{3}{2}} \left[\pi + 2 \sin^{-1} \sqrt{\frac{\xi_0^2}{2}} - \frac{2}{3} \sqrt{2(s-l)} \right]$	$\frac{1}{\sqrt{\mu}} \left[\frac{(n+D)\Delta_1}{2} \right]^{\frac{3}{2}}$

Note: 1. $n \equiv r_2/r_1$ $2s \equiv r_1 + r_2 + l$.

2. I: low trajectory II: high trajectory.

3. Each inverse circular function refers to the smallest positive angle satisfying the defining equation.

REFERENCES

1. Plummer, H. C., An Introductory Treatise on Dynamical Astronomy, Cambridge Univ. Press, 1918, pp. 50-55.
2. Johnson, R. A., Advanced Euclidean Geometry, Houghton Mifflin Co., 1929, p. 32.
3. Battin, R. H., The Determination of Round-Trip Planetary Reconnaissance Trajectories, J. Aeronautics and Space Sci., Vol. 26, No. 9, Sept. 1959, pp. 545-567.
4. Wheelon, A. D., Free-Flight of a Ballistic Missile, ARS J., Vol. 29, No. 12, Dec. 1959, pp. 915-926.
5. Godal, Th., Conditions of Compatibility of Terminal Positions and Velocities, Proceedings XIth International Astronautical Congress, Stockholm, 1960, Springer-Verlag, Vol. I, pp. 40-44.
6. Sun, F. T., A Special Hodograph for Orbital Motion, 2nd International Symposium on Rockets and Astronautics, Tokyo, 1960.
7. Sun, F. T., Some Applications of the Special Hodograph for Orbital Motion, 3rd International Symposium on Rockets and Astronautics, Tokyo, Aug. 1961.
8. Sun, F. T., On the Hodograph Method for Solution of Orbit Problems, Proceedings 12th International Astronautical Congress, Washington, D.C., Oct. 1961, Academic Press, Vol. II, pp. 879-916.
9. Ehricke, K. A., Space Flight, Vol. II, Chapter 1, Nostrand, N. Y., 1962.